

Mixed order transition and condensation in exactly soluble one dimensional spin model

Amir Bar, David Mukamel

Department of Physics of Complex Systems, Weizmann Institute of Science,
Rehovot 7610001, Israel

E-mail: amir.bracha@weizmann.ac.il, david.mukamel@weizmann.ac.il

Abstract. Mixed order phase transitions (MOT), which display discontinuous order parameter and diverging correlation length, appear in several seemingly unrelated settings ranging from equilibrium models with long-range interactions to models far from thermal equilibrium. In a recent paper [1] an exactly soluble spin model with long-range interactions that exhibits MOT was introduced and analyzed both by a grand canonical calculation and a renormalization group analysis. The model was shown to lay a bridge between two classes of one dimensional models exhibiting MOT, namely between spin models with inverse distance square interactions and surface depinning models. In this paper we elaborate on the calculations done in [1]. We also analyze the model in the canonical ensemble, which yields a better insight into the mechanism of MOT. In addition, we generalize the model to include Potts and general Ising spins, and also consider a broader class of interactions which decay with distance with a power law different from 2.

<i>CONTENTS</i>	2
Contents	
1 Introduction	3
2 Mixed order transitions (MOT) in one dimension	4
2.1 The inverse distance squared Ising (IDSI) model	4
2.2 The Poland-Scheraga (PS) model	5
3 TIDSI model	7
3.1 Definition	7
3.2 Summary of results	9
3.2.1 Phase diagram	9
3.2.2 Free energies	10
3.3 Comparison with the PS and IDSI models	13
3.3.1 PS model	13
3.3.2 IDSI model	14
4 Grand canonical analysis	14
4.1 The normal phase	15
4.2 Appearance of condensate in the low temperature phase	17
4.3 Condensate phase - regularization	17
5 Canonical analysis	18
5.1 Large deviations functions	18
5.1.1 Magnetization large deviations function F_M	18
5.1.2 Domains density large deviations function F_N	21
5.2 Finite size corrections	22
5.2.1 Corrections to Z_N	22
5.2.2 Corrections to Z_M	23
6 RG analysis	23
6.1 Model definition	24
6.2 RG analysis	24
6.3 Comparison with the flow diagram of IDSI and related models	26
7 Generalizations	27
7.1 General interactions decay law	27
7.1.1 Definition	27
7.1.2 Analysis	27
7.2 General spins	28
7.2.1 Potts spins	29
7.2.2 General Ising spins	30
8 Conclusions	31
Appendix A Analysis of the LHS of Eq.(49)	32
Appendix B Approximating (45) without saddle point	33
B.1 Deriving Eqs.(92-93)	34
Appendix C Approximating (54) without saddle point	35

Appendix D Numerical procedure for evaluating the partition function 36**1. Introduction**

Classification of phase transitions is a narrative in statistical physics and quantum field theory. A common starting point is the distinction between first order transitions and continuous - or critical - transitions. While in first order transitions the order parameter is discontinuous, or more generally the free energy is non-differentiable, in continuous transitions the order parameter changes continuously and the free energy is non-analytic but has a first derivative. Continuous transitions are known to possess universal features and can thus be categorized into universality classes, as opposed to first order transitions which are non-universal. The universality of critical transitions is tightly related to the divergence of a correlation length. Much progress has been made in classifying critical transitions based on methods such as renormalization group and conformal field theory which rely on such divergence.

However, there are known examples that deviate from the above scheme, for instance transitions for which on the one hand the free energy is non-differentiable but on the other hand they display a diverging correlation length [2]. Early examples of such mixed order transitions (MOT) include (a) one dimensional discrete spin models with long-range interactions [3, 4, 5, 6, 7, 8], and (b) models of depinning transitions such as models of DNA denaturation [9, 10] and of wetting [11, 12]. More recently there has been renewed interest in MOT taking place in studies of percolation models in the context of glass and jamming transitions [13, 14, 15, 16, 17], evolution of complex networks [18, 19, 20, 21] and active biopolymer gels [22]. While all these examples exhibit MOT, they display some qualitative and quantitative differences. For instance the divergence of the correlation length is algebraic in some of them, while it is a stretched exponential in others. It would be interesting to understand the origin of the similarities and differences between the various models by studying them within a common framework.

In [1] a new model which establishes a link between the classes of models (a) and (b) was introduced and analyzed, thus making a step towards a unified view. Specifically, this study focuses on two specific representative models of classes (a) and (b): The one dimensional Ising model with interactions decaying with the distance r between spins as r^{-2} (dubbed IDSI, for inverse distance squared Ising model) [4, 23, 7] and the Poland Scheraga (PS) model for DNA denaturation [9, 24]. The first class exhibits a Kosterlitz-Thouless (KT) vortex unbinding like transition [25], while the second class exhibits a condensation transition similar to the Bose Einstein condensation (BEC) transition of free bosons. The model presented in [1], which we shall refer to as the Truncated IDSI (TIDSI) model, thus provides an intriguing connection between KT and BEC transitions in one dimension. Another appealing property of the TIDSI model is that it is exactly soluble.

In this paper we extend the analysis of [1] in several directions:

- The calculations done in [1] are elaborated, and many features of the phase diagram which were only briefly mentioned in [1] are derived explicitly.
- The exact free energies of different ensembles are derived. These shed new light on the origin of criticality in the mixed-order transition appearing in the TIDSI model.

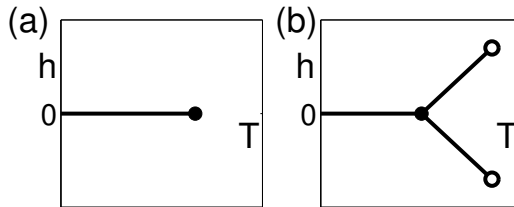


Figure 1. Schematic phase diagrams of (a) the IDS model defined by Eq.(1), and (b) the Blume-Capel model defined by Eq.(2).

- We generalize the model to include spins other than Ising spins, so that these models could be compared with models of class (a) other than the IDS [6]. We also consider long-range interactions decaying as $r^{-\alpha}$, with $\alpha \neq 2$.

The paper is organized as follows: we start in section 2 by reviewing MOT in one dimension and describe in detail the IDS and PS models. Then in section 3 the TIDS model is presented, and the relation to the IDS and PS model is discussed. We also summarize in this section the main results of the paper, including the phase diagram and the free energies. The next three sections are dedicated to deriving these results using grand canonical analysis (section 4), canonical analysis (section 5) and renormalization group (RG) analysis (section 6). While the TIDS model is exactly soluble, the IDS model is not, but as we show in section 6 the RG analysis can be used as a common framework for studying both models. The TIDS model is then extended to include more general interactions (section 7.1) and other spin variables (section 7.2).

2. Mixed order transitions (MOT) in one dimension

In this section we briefly review two models exhibiting MOT in one dimension. As mentioned above these models are prototypical representatives of wider classes of models.

2.1. The inverse distance squared Ising (IDS) model

The IDS is a one dimensional Ising model with long-range interactions which decay asymptotically as r^{-2} where r is the distance between the spins. Formally it is defined on a one dimensional lattice of size L , where in each lattice site there is a spin variable $\sigma_i = \pm 1$, and the Hamiltonian is

$$H = - \sum_{i < j} J(i-j) \sigma_i \sigma_j \quad ; \quad J(r \gg 1) \sim r^{-2}, \quad (1)$$

with $J(r) \geq 0$ for all r . More generally, one can consider interactions decaying as $J(r \gg 1) \sim r^{-\alpha}$. It has been proved by Ruelle [26] and Dyson [27] that $\alpha = 2$ is a borderline case, i.e. that models with $\alpha > 2$ exhibit no phase transition, while models with $1 < \alpha < 2$ show a symmetry breaking transition at some finite critical temperature $T_c > 0$. Models with $\alpha \leq 1$ have non-extensive energy and hence they are ordered at all temperatures. We shall henceforth refer to the $\alpha = 2$ case as the inverse distance squared Ising (IDS) model. Thouless, through an entropy-energy argument,

has suggested that the IDSI model exhibits a unique phase transition in which the magnetization exhibits a discontinuity at the critical temperature [4]. Dyson proved the existence of such a transition, (where the discontinuity of the order parameter is dubbed the “Thouless effect”), in a hierarchical version of the model [5]. A scaling analysis carried out by Anderson et al. [23] and a later Renormalization group (RG) analysis done by Cardy [6], showed that the transition in the IDSI model is of the Kosterlitz-Thouless (KT) type [25], with correlation length which diverges at the transition with an essential singularity as $\xi \sim \exp(1/\sqrt{T-T_c})$. The rigorous proof for the existence of the transition in the IDSI model was given only in the 1980’s by Frohlich and Spencer [28], while the mixed order nature of the transition was proved substantially later by Aizenman et al. [7]. A numerical validation for the analytical predictions was given in [29, 30].

The phase diagram of the IDSI model in the temperature-magnetic field (T, h) plane is given in Fig.1a. It resembles the $d > 1$ dimensional Ising model phase diagram, with a low-temperature first order transition at zero magnetic field h , which terminates at a critical point at $T_c > 0$. The only qualitative difference is that at $T = T_c$ the transition of the IDSI is discontinuous, that is the order parameter — the magnetization — jumps from 0 at $T = T_c^+$ to $\pm m_c \neq 0$ at $T = T_c^-$. However, the transition, as mentioned above, is still critical as there is a diverging correlation length. This is different from more common first order symmetry breaking transitions, as is found, for instance, in Blume-Capel model

$$H = -J \sum_{i \neq j} \sigma_i \sigma_j + \Delta \sum_i \sigma_i^2 - h \sum_i \sigma_i \quad ; \quad \sigma_i \in \{-1, 0, 1\}. \quad (2)$$

in a certain range of the parameters J and Δ and at $h = 0$.

A schematic temperature-magnetic field phase diagram for the Blume-Capel model for fixed J and Δ is presented in Fig.1b. Here the $T = T_c, h = 0$ point is actually a triple point in which three first order lines meet, i.e. in which three phases coexist. These are the + phase, the − phase and the disordered phase. There are also finite h transition lines on which there is a coexistence of two magnetically ordered phases. These finite h lines terminate in a usual second order critical point [2].

Although the main features of the phase diagram of the IDSI model have been proven rigorously [28, 7], there are many missing details: Non-universal quantities such as the critical temperature are not known exactly. The free energy of the model was not calculated, and clearly the partition function cannot be calculated in any ensemble. The model which is analyzed in this paper is a modified version of the IDSI in which all of these quantities can be exactly calculated.

2.2. The Poland-Scheraga (PS) model

The PS model is a model of DNA denaturation [9]. Denaturation is the process in which the two strands of the double-stranded DNA molecule separate upon heating. The PS model idealizes the DNA molecule as an alternating chain of bound segments and denatured loops as depicted in Fig.2. For homopolymers, while a bound segment of length l contributes an energy $-\epsilon l$, $\epsilon > 0$ being the binding energy of DNA base-pairs, loops are assumed to contribute no energy, but they contribute entropy S of the form $e^S \approx \omega \frac{s^l}{l^c}$, where ω and s are some non-universal constants and c is a universal exponent termed the *loop exponent*. Thus

$$S(l) = bl - c \log(l) + \tilde{\Delta}, \quad (3)$$

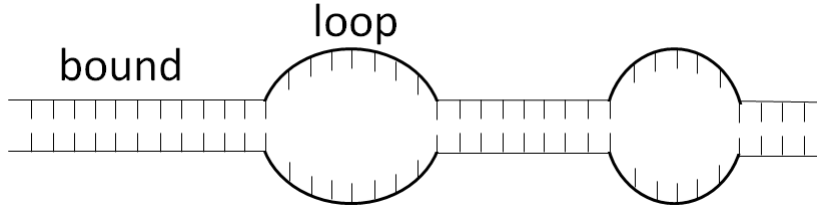


Figure 2. A typical configuration of the PS model

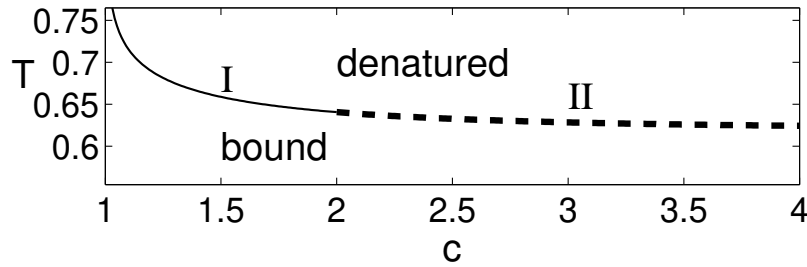


Figure 3. Phase diagram of the PS model.

with $b \equiv \log(s)$ and $\tilde{\Delta} \equiv \log(\omega)$. This form emerges from modeling the denatured loop as a closed path [10], which results in a universal exponent c that depends only on dimensionality and topological constraints, i.e. whether the path is considered as an ideal walk, self avoiding walk etc. [24]. The order parameter for this system is the fraction of bound base-pairs θ , with $\theta = 0$ above the melting temperature T_c , and is positive below T_c . The nature of the transition depends on the exponent c , as depicted in the phase diagram in Fig.3: For $c \leq 1$ the strands are bound at all temperatures and $T_c = \infty$. For $1 < c \leq 2$ there is a continuous transition at $T = T_c$ with $\theta \rightarrow 0$ as $T \rightarrow T_c$. For $c > 2$ the order parameter is discontinuous, i.e. $\theta \rightarrow \theta_c > 0$ as $T \rightarrow T_c$. For all $c > 1$ the correlation length ξ diverges at the transition point as $\xi \sim (T - T_c)^{-\nu}$ with $\nu = \max\left\{\frac{1}{c-1}, 1\right\}$, and hence for $c > 2$ the transition is of MOT type. The mechanism of the transition is mathematically similar to the Bose-Einstein condensation (BEC) transition in non-interacting Bose gas, with the condensate being the macroscopic loop formed at the transition temperature T_c .

There are several clear differences between the MOT transition in the PS model and in the IDSI model. First, the correlation length in the two models diverges differently: algebraically in the PS model and as a stretched exponential in the IDSI model. Within a renormalization group analysis, the PS model displays a one-parameter family of fixed points with continuously varying exponent while the transition in the IDSI is controlled by a single fixed point. In addition, the PS transition is a condensation transition which is characterized by the formation of a single macroscopic loop. No such macroscopic object is associated with the IDSI transition. Finally, while the IDSI transition is a symmetry breaking transition, there is no symmetry which is broken in the PS case. To understand the origin of the similarities and differences between these two models — and between the classes they represent — we introduced in [1] the TIDSI model which serves as a bridge between

these models. We now turn to define the model and show explicitly its similarity to those two models.

3. TIDSI model

3.1. Definition

Like the IDSI model, the TIDSI model of [1] is defined on a one dimensional Ising chain, where on each site i there is a spin variable $\sigma_i = \pm 1$. The interaction between spins is composed of a nearest neighbor interaction term $-J_{NN}\sigma_i\sigma_{i+1}$ and a long-range interaction term $-J(i-j)\sigma_i\sigma_j I(i \sim j)$, where $I(i \sim j) = 1$ if sites i and j are in the same domain of either all up or all down spins, and $I(i \sim j) = 0$ otherwise. Thus the long-range interactions (beyond nearest neighbors) are confined within each of the domains. As in the IDSI model we take the interaction strength $J(r)$ to decay as r^{-2} . The indicator function $I(i \sim j)$ can be written explicitly in terms of the spin variables

$$I(i \sim j) = \prod_{k=i}^{j-1} \delta_{\sigma_k \sigma_{k+1}} = \prod_{k=i}^{j-1} \frac{1 + \sigma_k \sigma_{k+1}}{2}.$$

Hence the resulting Hamiltonian reads

$$H = -J_{NN} \sum \sigma_i \sigma_{i+1} - \sum_{i < j} J(i-j) \sigma_i \sigma_j \prod_{k=i}^{j-1} \frac{1 + \sigma_k \sigma_{k+1}}{2}, \quad (4)$$

which explicitly contains multi-spin interactions of arbitrary order. For concreteness we take $J(r) = Cr^{-2}$ for $r \geq 1$, even though the results are qualitatively the same for any $J(r)$ which has the same asymptotic form.

An alternative representation of a configuration of the model is in terms of domains: Each microscopic configuration is defined in terms of the spin at the first site σ_1 , the number of domains $1 \leq N \leq L$ and their lengths $\{l_a\}_{a=1}^N$ where $l_a \geq 1$ and $\sum_a l_a = L$. Due to the truncation of the long-range interactions to within domains, the energy (4) can straightforwardly be expressed in terms of these variables: The nearest neighbors term sums up to

$$H_{NN} = -J_{NN} [(L-1) - 2(N-1)] = 2J_{NN}N - J_{NN}(L+1), \quad (5)$$

while the energy contribution of the long-range term for each domain $H_{LR}(l)$ is given by

$$\begin{aligned} H_{LR}(l) &= -C \sum_{k=1}^l \frac{l-k}{k^2} = -C \left[l \left(\zeta_2 - \frac{a}{l} + O(l^{-2}) \right) - \log(l) + O(l^{-1}) \right] \\ &= -bl + C \log(l) + \tilde{\Delta} + O(l^{-1}), \end{aligned} \quad (6)$$

where $\zeta_2 \equiv \sum_{k=1}^{\infty} k^{-2}$, $a > 0$ is an expansion coefficient, $b \equiv C\zeta_2$ and $\tilde{\Delta} \equiv Ca$. Eq.(6) is of the same form as $-TS(l)$ where S is the loop entropy in the PS model given in Eq.(3), under the mapping $c \rightarrow \beta C$ where $\beta = T^{-1}$ (we use units in which the Boltzmann constant k_B is unity). In essence, the physics of both models stem from the logarithmic dependence of the energy (entropy) on the domain (loop) length. The mapping between energy and entropy implies an inversion of the temperature role, and hence of a mapping between the high temperature phase of the PS model and the low temperature phase of the TIDSI model. Other than this trivial difference, the

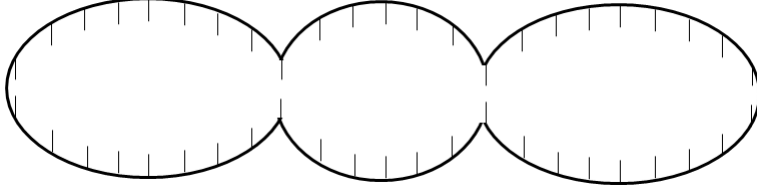


Figure 4. An illustration of the TIDSI model as a symmetric PS model, where all spin are within loops (domains) and none are in bound segments (compare to Fig.2).

phenomenology of the two models is almost identical. The only qualitative difference between the phase diagrams of the two models is due to the additional spin inversion symmetry which exists in the TIDSI model and is lacking in the PS model, as will be discussed below. Another important difference is that while the parameter c in the PS model is a universal exponent, for the TIDSI model the corresponding parameter $\beta_c C$, with $\beta_c = T_c^{-1}$, depends on the details of the model such as the nearest-neighbors coupling J_{NN} .

Neglecting terms of order $O(l^{-1})$ and combining (5) and (6), the Hamiltonian expressed by the domains variables reads

$$H(N; \{l_n\}) = H_{NN} + \sum_n H_{LR}(l_n) = \Delta N + C \sum_n \log(l_n) + \text{Const}, \quad (7)$$

where $\Delta \equiv \tilde{\Delta} + 2J_{NN} > 0$. The constant term in (7), which contains also expressions like $-J_{NN}L$, can be set to 0 without loss of generality, and this will be our convention henceforth. In terms of the mapping to the PS model, the Hamiltonian (7) can be viewed as the log-Boltzmann factor of a configuration made up of a sequence of loops without bound segments in between, as depicted in Fig.4. Hence the TIDSI model can be viewed either as a truncated version of the IDSI model or as a symmetrized version of the PS model.

The transition in the TIDSI model can be described using two order parameters: first, the magnetization $m = \frac{1}{L} \sum \sigma_i$, which in the domains variables reads

$$m = -\frac{\sigma_1}{L} \sum_{a=1}^N (-1)^a l_a. \quad (8)$$

The second order parameter is the density of domains $n \equiv \frac{N}{L}$. A magnetic field h can be added to the Hamiltonian (7) by adding a term $-hM$ where $M \equiv Lm$, and similarly a loop chemical potential μ can be added as $-\mu N$.

Finally, we should define the statistical ensemble which we shall focus on. Both the IDSI and PS models are defined in the canonical ensemble in which the length of the chain L is fixed. The partition function of the TIDSI model in this ensemble can be written in terms of the domains variables as

$$Z_C(L; \beta) = \sum_{N=1}^{\infty} \sum_{l_1=1}^{\infty} \dots \sum_{l_N=1}^{\infty} e^{-\beta H} I\left(L = \sum_{a=1}^N l_a\right), \quad (9)$$

with H given by (7) and the indicator function $I(\psi) = 1$ if ψ is true and is 0 otherwise. However, we also consider more restricted ensembles in which either the magnetization M or number of domains N or both are fixed. The free energies in such ensembles play

a similar role of a Landau free energy, enabling deeper understanding of the nature of the transition, as we discuss below. The partition function in the ensemble in which both M and N are fixed reads

$$Z_0(L, M, N; \beta) = \sum_{\{l_a\}} e^{-\beta H} I\left(L = \sum l_a\right) I(M = Lm(\{l_a\})). \quad (10)$$

From this partition function we can derive the marginal partition sums

$$Z_M(L, M; \beta) = \sum_N Z_0(L, M, N; \beta), \quad (11)$$

$$Z_N(L, N; \beta) = \sum_M Z_0(L, M, N; \beta), \quad (12)$$

$$Z_C(L; \beta) = \sum_{M, N} Z_0(L, M, N; \beta). \quad (13)$$

3.2. Summary of results

In this section we present a summary of the results derived for the TIDSI model in sections 4 and 5. As stated above, the transition in the TIDSI model is quite similar to the transition of the PS model (only the role of temperature is inverted): The high temperature phase of the TIDSI model is composed of a gas of microscopic (finite size) domains, while the low temperature phase consists essentially of a single macroscopic domain. The transition is then a condensation transition, it is MOT for zero magnetic field but can be either continuous or MOT for nonzero field, as discussed in details in the next subsection. In addition to calculating exactly the phase diagram, we calculated the free energies of the model in ensembles in which either the magnetization or the density of domains are fixed. These free energies play the role of the Landau free energies in some sense, and hence allow a deeper understanding of the behavior of the system, as discussed in subsection 3.2.2.

3.2.1. Phase diagram The phase diagram of the TIDSI model is presented in Fig.5. Fig.5a displays the transition temperature (T_c) as a function of the coupling c at $h = 0$. Here

$$c \equiv \beta_c C,$$

where $\beta_c = T_c^{-1}$ and T_c is the critical temperature. The transition line is given by

$$\zeta(\beta_c C) = e^{\beta_c \Delta}, \quad (14)$$

where $\zeta(z)$ is the Riemann Zeta function. The high temperature phase is disordered. Hence the average magnetization vanishes, $\langle m \rangle = 0$, and the number of domains is macroscopic $\langle n \rangle > 0$. For $T < T_c$, the phase is ordered, but unlike spin models with two-body interactions, the magnetization is saturated, i.e. $\langle m \rangle = \pm 1$ throughout the low temperature phase. In addition $\langle n \rangle = 0$ as there is essentially a single macroscopic domain. This jump between zero to saturated magnetization is an extreme example of the Thouless effect. As mentioned above, the Thouless effect — first conjectured to take place in the IDSI model — refers to a transition in which the magnetization is discontinuous while the correlation length diverges. In considering the other order parameter $\langle n \rangle$, one finds that the nature of the transition changes along the transition line: for $1 < c \equiv \beta_c C \leq 2$ (region I) the average density of the domains $\langle n \rangle$ drops continuously to 0; for $2 < c \leq 3$ (region II) there is a discontinuity in $\langle n \rangle$ from a

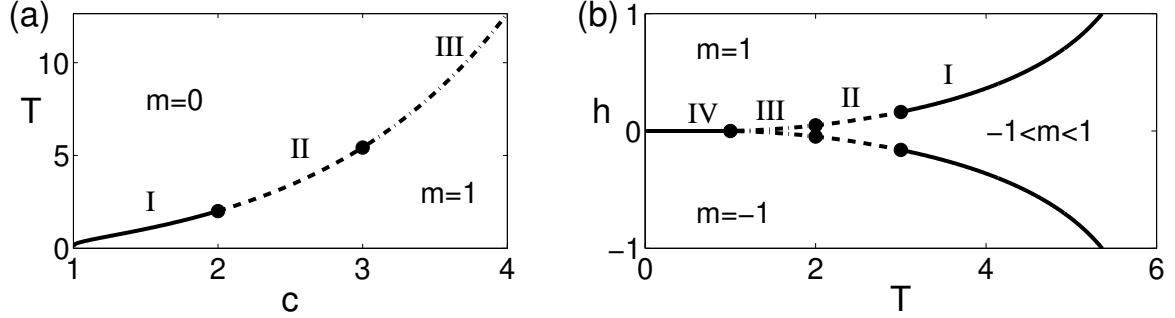


Figure 5. Phase diagram of the TIDSI model: (a) the (c, T) projection, with $\Delta = 1$; and (b) the (T, h) projection for $c = C = 6$ and $\Delta = \log \zeta_c$ so that $T_c(h=0) = 1$. The different regions (I-IV) are explained in the text.

finite density of domains n_c to 0 at the transition, but the magnetic susceptibility $\chi_0 \equiv \frac{\partial^2 \log Z_C}{\partial h^2} \Big|_{h=0}$ diverges as $T \searrow T_c$; for $c > 3$ (region III) the density of domains $\langle n \rangle$ is discontinuous and χ_0 is finite. For any $c > 1$ the correlation length ξ diverges as

$$\xi \sim (T - T_c)^{-\nu} \quad ; \quad \nu = \max \left(1, \frac{1}{c-1} \right). \quad (15)$$

The mechanism of the transition is similar to that of the Bose-Einstein condensation (BEC): while above the critical temperature there is an extensive number of microscopic domains, which can be referred to as a normal gas of domains, below T_c there is a single macroscopic domain, which can be referred to as the condensate.

In Fig.5b the phase diagram in the (T, h) plane is plotted. The transition lines in the (T, h) diagram are given by

$$\zeta(\beta_c C) \Phi_{\beta_c C} \left(e^{-2\beta_c |h|} \right) = e^{2\beta_c \Delta}, \quad (16)$$

where $\Phi_\gamma(u)$ is the Polylogarithm function, which satisfies $\Phi_\gamma(1) = \zeta(\gamma)$. Each of the two transition lines at finite h separates two phases: The gas phase where $-1 < \langle m \rangle < 1$ and $\langle n \rangle > 0$, and the condensed phases where $\langle n \rangle = 0$ and $\langle m \rangle = 1$ or $\langle m \rangle = -1$. The nature of the transition changes along the transition line: for $c(h) \equiv \beta_c(h)C > 3$ (region III) there is a diverging length scale, finite susceptibility and discontinuous $\langle m \rangle$ and $\langle n \rangle$. For $2 < c(h) \leq 3$ (region II) the susceptibility becomes divergent. For $1 < c(h) \leq 2$ (region I) the susceptibility diverges and the transition is continuous both in $\langle n \rangle$ and $\langle m \rangle$. This is unlike the $h = 0$ case, in which the magnetization is discontinuous. For $T < T_c(h)$ the transition line between the two condensed phases (region IV) is a normal first order transition as in short-range Ising models (in $d \geq 2$).

3.2.2. Free energies In addition to the phase diagram, the logarithm of the partition function was evaluated to leading and next to leading order in L^{-1} . The leading order term is just the free energy, or more generally the large deviations function (LDF) [31]. The next to leading order (finite size correction) provides an insight into the mechanism of the transition, revealing a logarithmic (in L) barrier between coexisting phases, which implies that the fluctuations of the order parameters decay as a power-law and hence are critical.

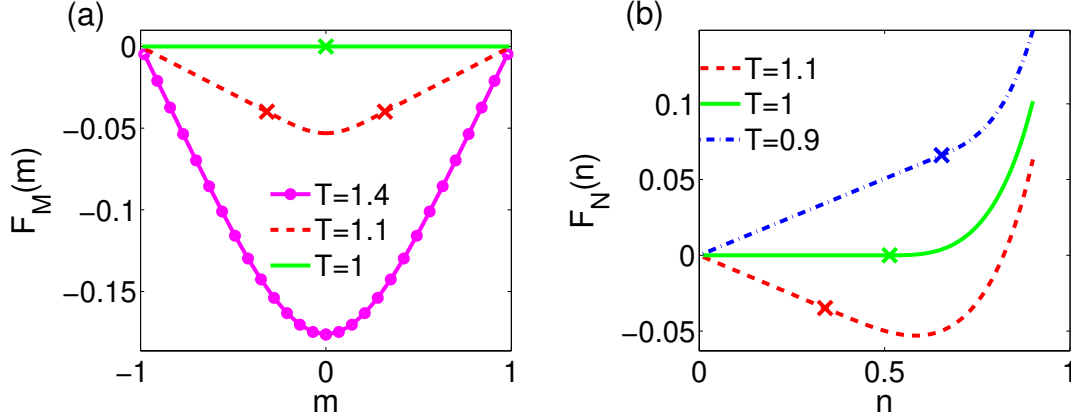


Figure 6. (color online) Free energies of the (a) constant magnetization ensemble, and (b) constant number of domains ensemble. The X marks correspond to $\pm m_c$ in (a) and n_c in (b), as defined in the text. Notice that in (a) for $T = 1.4$ there is no X mark as $m_c = 1$, and for $T = 1$ there is a single X mark as $m_c = 0$. The parameters used to produce these figures and the following ones are $c = 2.5$ and $\Delta = \log \zeta_c \approx 0.29$ so that $T_c = 1$.

Large Deviations functions The LDF for the magnetization in zero external magnetic field is given by

$$\begin{aligned} F_M(m; \beta) &\equiv - \lim_{L \rightarrow \infty} \frac{1}{L} \log Z_M(L, mL; \beta) \\ &= \left(\frac{1+m}{2} \right) \log [z_+^*] + \left(\frac{1-m}{2} \right) \log [z_-^*], \end{aligned} \quad (17)$$

where, for $m \geq 0$, z_{\pm}^* are given by

$$z_-^* = W_- (z_+^*, \beta), \quad (18)$$

$$z_+^* = \begin{cases} W_+(m, \beta) & m < m_c \\ 1 & m \geq m_c \end{cases}, \quad (19)$$

with W_- and W_+ are given implicitly by Eq. (44) and Eq.(48) respectively. Since F_M is symmetric in m , this sets its value also for $m < 0$. Here W_{\pm} are analytic (and non-constant) functions of their arguments, and $W_+(m_c, \beta) = 1$, where $m_c = 1$ for $\beta C \leq 2$, while it is a decreasing function of β which vanishes at β_c given by Eq.(14). This implies that if $c \equiv \beta_c C > 2$, then for a given β in the interval $[\frac{2}{C}, \beta_c]$, the LDF is linear for $|m| > m_c$, as can be seen in Fig.6a. This linearity is the usual Maxwell construction of a first order transition in which under a magnetization constraint, the system phase separates and hence the free energy is essentially the weighted sum of the corresponding free energies of the phases. In this case the phases are the normal gas of domains with $|m| = m_c$ and the condensate with $|m| = 1$. There are obviously two symmetric condensates, with $m = \pm 1$, and well below the critical temperature, when the gas phase becomes unstable, the coexistence is between those two condensates, and hence the free energy is completely flat. Note that detailed characterization of the nature of the phase transition requires the knowledge of the L^{-1} correction to the free energy, which will be presented below.

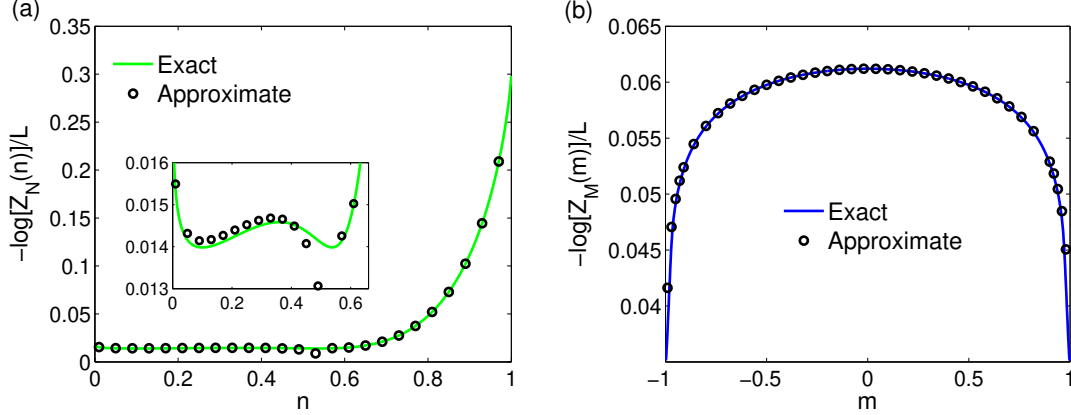


Figure 7. (color online) Exact numerical evaluation ($L = 1000$) vs. analytical approximation (a) for $-\frac{1}{L} \log Z_N$ slightly below T_c ($T = 0.95T_c$), and (b) for $-\frac{1}{L} \log Z_M$ for $T = 0.5T_c$.

The LDF of the domains density is given by

$$\begin{aligned} F_N(n; \beta) &\equiv - \lim_{L \rightarrow \infty} \frac{1}{L} \log Z_N(L, nL; \beta) \\ &= \log z^* - n \log [e^{-\beta \Delta} \Phi_{\beta C}(z^*)], \end{aligned} \quad (20)$$

where z^* is given by

$$z^* = \begin{cases} W_n(n, \beta) & n > n_c \\ 1 & n \leq n_c \end{cases}, \quad (21)$$

with W_n is given implicitly by Eqs.(56). Here W_n is an analytic function of its arguments such that $W_n(n, \beta) \leq 1$ for $n > n_c$, and it is an increasing function of n so that equality is achieved only for $n = n_c$. In addition, $n_c = 0$ for $\beta C \leq 2$, it is an increasing function of β and it tends to 1 for $\beta \rightarrow \infty$. Thus, as for F_M , we find that F_N has a linear part for $0 < n < n_c$ and $c > 2$. It can also be seen that at the critical temperature, given by (14), the slope of the linear part of F_N vanishes, while it is negative for $\beta < \beta_c$ and positive for $\beta > \beta_c$ (see Fig.6b). This implies that the minimum of the free energy is at $n^* > n_c$ for $\beta < \beta_c$, at $n^* = 0$ for $\beta > \beta_c$, and is degenerate on the interval $[0, n_c]$ for $\beta = \beta_c$. Hence for $c > 2$ we find indeed a discontinuous change of $\langle n \rangle$ at the transition, while for $c \leq 2$ the change is continuous as $n_c = 0$ at the transition.

Finite size corrections Fig.7 presents an exact numerical calculation (see Appendix D) and analytic approximation (see section 5.2) to $-\frac{1}{L} \log Z_N$ and $-\frac{1}{L} \log Z_M$ for a finite system of size $L = 1000$. Fig.7a shows that the transition is indeed first-order-like, with the usual picture of two competing wells, and that the linearity of the LDF comes from a Maxwell construction. In both figures 7a-b it can be seen that the approximations Eq.(60-62) are quite accurate. An immediate application of having an explicit approximation is the observation that the free energy barriers, which suppress fluctuations of the order parameters, are logarithmic in L and n . Hence fluctuations are distributed following a power law, which implies divergence of the correlation length and criticality.

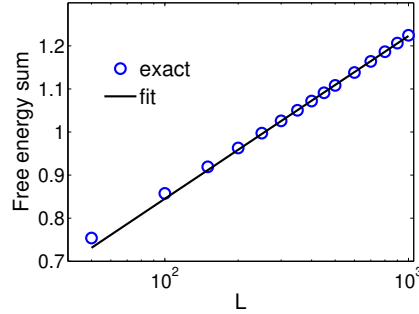


Figure 8. Scaling of $R(L)$ with L . The linearity of the graph on a semi-logarithmic scale shows the logarithmic scaling, i.e. $R(L) \sim \log L$.

This analytical observation is verified by an exact numerical analysis presented in Fig.8, in which the weight of fluctuations of the density of domains n at T_c are quantified. This is done by calculating the sum of the free energy of such fluctuations from $n = 0$ to the minimum of the free energy at n^*

$$R(L) \equiv \int_0^{n^*} -\log Z_N(L, Ln; \beta) dn. \quad (22)$$

From Eq.(60-61) it is evident that there is a unique minimum of the free energy at $n^*(L) > n_c$, which represents a gas of domains. In Fig.8 it is shown that $R(L)$ scales logarithmically with L , implying logarithmic free energy barriers.

3.3. Comparison with the PS and IDSI models

As was shown above, the TIDSI model can be considered as a symmetric version of the PS model or as a truncated version of the IDSI model. In this section we discuss the similarities and differences in the phenomenology of the three models.

3.3.1. PS model The TIDSI model has a very similar phase diagram to that of the PS model, as can be appreciated by comparing Fig.3 and Fig.5a, recalling the inverted role of the temperature in the two models. Essentially the mechanism of the phase transition is the same, i.e. a condensation transition in which a single domain - or a single loop - becomes macroscopic and encompasses the whole system. There are a few differences, though, which we shall discuss now.

The most important difference is that at $h = 0$, the TIDSI model exhibits an extreme transition in magnetization, from $m = 0$ to $m = \pm 1$. This also happens for $1 < c \leq 2$, for which the PS model exhibits a second order transition. The reason for this difference is the symmetry between $+$ and $-$ spins in the TIDSI model, which is lacking in the PS model. Due to this symmetry, the magnetization vanishes above the transition (as long as there is no magnetic field). To break the symmetry there must be either an external symmetry breaking field or a spontaneous symmetry breaking transition. Note that once a symmetry breaking field is applied, the transition becomes almost identical to the PS transition, as for $1 < c(h) \leq 2$ the transition is second order. A second related difference is the existence of two order parameters which behave differently for $1 < c \leq 2$: the density of domains, n , which is continuous

and the magnetization which is discontinuous. This has to do with the symmetry of the model under magnetization reversal, which has no counterpart for the n order parameter. Hence the behavior of n in the TIDSI model is the same as that in the PS model.

Another difference has to do with the parameter c . In the PS model this parameter is the universal exponent controlling the number of configurations of a self-avoiding random loop. The value of c is hence independent of geometry and depends only on the spatial dimension and topological constraints. In the TIDSI model, on the other hand, the parameter C itself is rather arbitrary, and moreover the value of the critical temperature β_c depends both on C and on Δ , or the nearest neighbors interactions. Hence $c \equiv \beta_c C$ depends on the model parameters rather than being universal.

3.3.2. IDSI model The main similarity between the IDSI model and the TIDSI model is that both exhibit a mixed order symmetry breaking phase transition. There are, however, some distinctions between the two models. While the TIDSI has a finite magnetic field transition, the IDSI model exhibits no such transition, as expected from Ising ferromagnet with two body interactions by the Lee-Yang theorem [32, 33, 2]. Another difference is the divergence of length-scale at the transition, which is algebraic for the TIDSI model and essential singularity in the case of the IDSI model. The origin of this behavior is discussed in section 6 through the renormalization group analysis.

Perhaps a more fundamental difference between the models is the fact that in the IDSI there is no formation of a macroscopic domain (where a domain is defined as a consecutive set of spins all having the same sign). While the density of domains was not analyzed in the case of IDSI, it seems that it does not vanish for any finite temperature, though an interesting question is whether it is analytic at the transition or not. The lack of condensation in the IDSI is obviously the reason that the Thouless effect in this model is not extreme, i.e. that the magnetization jumps to a finite number < 1 .

4. Grand canonical analysis

We now establish analytically the results stated above. The model (7) is defined in the canonical ensemble where the chain length L is fixed. In an ensemble where L , N and M are fixed the partition function and the associated free energy (or large deviations function) are given by

$$Z_0(L, M, N; \beta) = e^{-\beta \Delta N} \sum_{l_1=1}^{\infty} \dots \sum_{l_N=1}^{\infty} \prod_{a=1}^N l_a^{-\beta C} I\left(L = \sum l_a\right) \times \\ I\left(M = -\sigma_1 \sum_{a=1}^N (-1)^a l_a\right), \quad (23)$$

$$F_0(M, N; \beta) = \lim_{L \rightarrow \infty} \frac{1}{L} \log Z_0(L, M, N; \beta) \quad (24)$$

As common in statistical mechanics, instead of evaluating the constrained partition sum (23) itself, we calculate the generating function

$$Q(p, h, \mu; \beta) = \sum_{L, M, N} Z_0(L, M, N; \beta) e^{L\beta p} e^{\beta h M} e^{\beta \mu N}. \quad (25)$$

For simplicity we assume symmetric boundary conditions with

$$\sigma_1 = 1 \quad ; \quad \sigma_L = -1, \quad (26)$$

which imply an even number of domains. Eqs.(23-26) yield

$$\begin{aligned} Q(p, h, \mu; \beta) &= \sum_N e^{-\beta(\Delta-\mu)N} \prod_{a=1}^N \left[\sum_{l=1}^{\infty} \frac{e^{\beta pl}}{l^{\beta C}} \exp((-1)^a \beta hl) \right] \\ &= \frac{e^{2\beta(\mu-\Delta)U(p+h)U(p-h)}}{1 - e^{2\beta(\mu-\Delta)U(p+h)U(p-h)}}, \end{aligned} \quad (27)$$

with

$$U(x) = \sum_l \frac{e^{\beta xl}}{l^{\beta C}} = \Phi_{\beta C}(e^{\beta x}). \quad (28)$$

The function $\Phi_\gamma(u)$ is the polylogarithm function, which has the following properties:

- (i) $\Phi_\gamma(u)$ is analytic in the complex plane except for a branch-cut along $[1, \infty)$
- (ii) $\Phi_\gamma(1) = \infty$ for $\gamma \leq 1$ and $\Phi_\gamma(1) = \zeta(\gamma)$ for $\gamma > 1$ where $\zeta(\gamma)$ is the Riemann Zeta function.
- (iii) $\frac{d}{dx} \Phi_\gamma(e^x) = \Phi_{\gamma-1}(e^x)$
- (iv) Expanding around $x = 0$, $\Phi_\alpha(e^x) = \Gamma(1-\alpha)(-x)^{\alpha-1} + \sum_{k=0}^{\infty} \frac{\zeta(s-k)}{k!} x^k$, where $\Gamma()$ is the Gamma function.

We proceed by using (27) to derive the results discussed in section 3, namely the discontinuity of the magnetization, the divergence of the correlation length etc. Then we argue that the low temperature phase is characterized by a single macroscopic domain - a *condensate*. Finally we justify the derivation for the low temperature phase using a regularization argument.

4.1. The normal phase

The thermodynamic behavior of the system is determined by the grand potential [12, 1]

$$p^* = \min_{M,N} \left\{ F_0(M, N) - h \frac{M}{L} - \mu \frac{N}{L} \right\}, \quad (29)$$

The average of the order parameters $m \equiv M/L$ and $n \equiv N/L$ are given by

$$\langle m \rangle = -\frac{\partial p^*}{\partial h} \quad ; \quad \langle n \rangle = -\frac{\partial p^*}{\partial \mu}. \quad (30)$$

According to Eq.(25), $e^{\beta p^*}$ corresponds to the singularity of Q closest to the origin (most negative p^*), as it is the radius of convergence of its defining series. Inspecting (27) we see that the singularity can stem either from the denominator becoming 0, i.e.

$$U(p^* + h)U(p^* - h) = e^{2\beta(\Delta-\mu)}, \quad (31)$$

or from the branch point of U , i.e.

$$p^* + |h| = 0. \quad (32)$$

In the analysis below we focus on the regime of small μ . For high temperatures, $\beta \rightarrow 0$, p^* is the solution of (31). By differentiating (31) with respect to h we find

$$m(h) = \frac{\Psi_+(p^*, h) - \Psi_-(p^*, h)}{\Psi_+(p^*, h) + \Psi_-(p^*, h)}, \quad (33)$$

$$\Psi_{\pm}(p, h) \equiv U'(p \pm h) U(p \mp h), \quad (34)$$

and hence $m \rightarrow 0$ for $h \rightarrow 0$ (as $\Psi_+(p, 0) = \Psi_-(p, 0)$). However, as β increases, the RHS of (31) increases (for $\Delta > \mu$) while the LHS decreases (for a given p^*) and hence p^* is an increasing function of β . Therefore there is a critical value of β such that Eq.(32) is also satisfied. This happens at β_c which is the solution of

$$\Phi_{\beta_c C}(1) \Phi_{\beta_c C}(e^{-2\beta|h|}) = e^{2\beta_c(\Delta - \mu)}. \quad (35)$$

From (35) it is clear that the parameter $c \equiv \beta_c C$ satisfies $c > 1$ since $\Phi_c(1)$ diverges for $c \leq 1$. As is described in section 4.3, below the transition, namely for $\beta > \beta_c$, the singularity of Q closest to the origin is given by Eq.(32), i.e. $p^* = -|h|$, and hence

$$m(h) = \text{sign}(h) \equiv \begin{cases} 1 & h > 0 \\ -1 & h < 0 \end{cases}. \quad (36)$$

Eq.(36) then proves the existence of a discontinuity of the magnetization, where $m(h \rightarrow 0)$ jumps from 0 to ± 1 at some finite β_c . In addition, we see from (33-36) that there is also a phase transition for $h \neq 0$, since while for $T > T_c$ the magnetization is given by (33) so that $0 < |m(h)| < 1$, for $T < T_c$ the magnetization is $m(h) = \text{sign}(h)$. The order of this transition depends on $U'(0)$: When it diverges the transition is continuous as can be verified from Eq.(33), while when it is finite the transition involves a discontinuity of the magnetization. From the properties of the polylogarithm function this implies that the magnetization is continuous for $c(h) \equiv \beta_c(h)C \leq 2$ and discontinuous for $c(h) > 2$.

Calculating the average N in the high temperature regime by differentiating (31) with respect to μ yields

$$n(h) = \frac{2\beta e^{2\beta(\Delta - \mu)}}{\Psi_+(p^*, h) + \Psi_-(p^*, h)}.$$

In the low temperature phase, where $p^* = -|h|$, the result is just $n = 0$. Hence n is continuous through the transition if $U'(0)$ diverges (and therefore also $\Psi_+(-|h|, h)$ or $\Psi_-(-|h|, h)$ diverge), i.e. $c \leq 2$, and is discontinuous otherwise. Thus the two order parameters m and n behave differently at $h = 0$. While m is discontinuous at the transition for any c , n is continuous for $1 < c \leq 2$ and discontinuous only for $c > 2$. On the other hand on the $h \neq 0$ transition lines both m and n change continuously for $c(h) \leq 2$ and jump for $c(h) > 2$.

One can also use the above results to calculate the magnetic susceptibility $\chi \equiv \frac{\partial m}{\partial h}$ and the distribution of domain sizes $P(l)$, which defines a typical length scale which diverges at the transition. Differentiating (33) with respect to h yields

$$\chi = \frac{2(\Psi_- \partial_h \Psi_+ - \Psi_+ \partial_h \Psi_-)(\Psi_+ + \Psi_-) + 2(\Psi_+ - \Psi_-)(\Psi_+ \partial_p \Psi_- - \Psi_- \partial_p \Psi_+)}{(\Psi_+ + \Psi_-)^3}. \quad (37)$$

As Ψ_{\pm} involve $U'(p^* \pm h)$, χ involves $U''(p^* \pm h)$. It is easy to see that there is no cancellation of these terms, and hence if $U''(0)$ diverges then χ diverges. From the properties of the Polylog it is evident that $U''(0)$ diverges if $c \leq 3$.

Finally, the distribution of the size of + and - domains is given by

$$\begin{aligned} P_{\pm}(l) &\simeq \frac{Z_C(L-l, h)}{Z_C(L, h)} \times \frac{e^{\pm\beta hl}}{l^{\beta C}} \\ &= \frac{e^{-\beta(p^* \pm h)l}}{l^{\beta C}} = \frac{e^{-l/\xi_{\pm}}}{l^{\beta C}}, \end{aligned} \quad (38)$$

where we used $Z_C \sim e^{-L\beta p^*}$ and defined $\xi_{\pm} \equiv [\log(p^* \pm h)]^{-1}$. The length scales ξ_{\pm} are not exactly the correlation length of the spin-spin correlation function, but they are lower bounds for it. For $h > 0$ ($h < 0$) the length scale ξ_+ (ξ_-) diverges as $T \rightarrow T_c$ for all c , which implies that the correlation length diverges as well. Expanding Eq.(31) near the transition, i.e. $t \equiv T - T_c \ll 1$, $\delta p \equiv -|h| - p^* \ll 1$, and using property 4 of the polylogarithm function we get

$$t \sim (\delta p)^{\gamma} \quad ; \quad \gamma = \min(c-1, 1).$$

The algebraic divergence of the correlation length Eq.(15) directly follows from this relation.

4.2. Appearance of condensate in the low temperature phase

In the low temperature phase, where $n = 0$, the number of domains in the system is sub-extensive. We argue that in fact this phase is composed of a single macroscopic domain by showing that this state is more favorable than having two condensates. The argument is similar to that given in [34] for condensation in the zero range process.

For a system with a single macroscopic domain and the boundary conditions (26), the partition sum scales as $Z_1 \sim L^{-\beta C}$. For a system with two macroscopic domains the partition function Z_2 is a sum of $O(L)$ terms, each represents a different location of the domain wall. Each term scales as $(L^{-\beta C})^2$ and hence $Z_2 \sim L^{1-2\beta C}$. In the low temperature phase $\beta C > 1$ and hence $-\beta C > 1 - 2\beta C$ and the single condensate state is preferable. This argument can be easily extended to other configurations of condensates. From the fact that there is a single condensate, one can easily deduce that $m = \pm 1$ in the low temperature phase.

4.3. Condensate phase - regularization

The above argument for the relation $p^* = -|h|$ in the low temperature phase is not mathematically justified, as the sum defining the grand partition function (25) is not well behaved in this regime.

One way to justify it is to invert the z-transform (25), thus finding Z_0 directly and validating (32) for $T < T_c$. This route is taken in section 5. Here we follow a different procedure, whereby the grand-canonical ensemble is regularized by introducing an upper cutoff to the domain length, thus making all quantities analytic, and then taking the upper cutoff to infinity. This procedure is well suited for models with a condensation phenomena (similar to BEC) and it was used in such context [35, 34, 36].

Let us consider the TIDSI model as defined in Eq.(7) and introduce an upper cutoff Λ on the domain length. The partition function for this modified model is

$$Q_{\Lambda}(p, h, \mu; \beta) = e^{\beta\Delta} \sum_N e^{-\beta(\Delta - \mu)N} \prod_{a=1}^N \left[\sum_{l=1}^{\Lambda} \frac{e^{\beta pl}}{l^{\beta C}} \exp((-1)^a \beta hl) \right]$$

$$= e^{\beta\Delta} \frac{e^{2\beta(\mu-\Delta)} U_{\Lambda}(p+h) U_{\Lambda}(p-h)}{1 - e^{2\beta(\mu-\Delta)} U_{\Lambda}(p+h) U_{\Lambda}(p-h)}, \quad (39)$$

with

$$U_{\Lambda}(x) = \sum_{l=1}^{\Lambda} \frac{e^{\beta x l}}{l^{\beta C}} = \Phi_{\beta C}^{\Lambda}(e^{\beta x}). \quad (40)$$

The function $\Phi_{\gamma}^{\Lambda}(u)$ is a truncated version of the polylogarithm, which is analytic for any u and γ . For given h and μ the thermodynamic limit $L \rightarrow \infty$ is again given by the most negative singularity of Q_{Λ} , i.e. by the solution of

$$U_{\Lambda}(p^* + h) U_{\Lambda}(p^* - h) = e^{2\beta(\Delta - \mu)}.$$

Since U_{Λ} is an analytic function, this equation has a solution for all β . Like before, p^* is an increasing function of β and therefore there is a temperature $\beta_c(\Lambda)$ for which $p^*(h, \mu, \beta_c(\Lambda)) = -|h|$. For $\beta > \beta_c(\Lambda)$ one has $p^* > -|h|$. In the limit $\Lambda \rightarrow \infty$, $\beta_c(\Lambda) \rightarrow \beta_c$ as given by Eq.(35). For any $u > 1$, $\lim_{\Lambda \rightarrow \infty} \Phi_{\beta C}^{\Lambda}(u) = \infty$, and hence for $\beta > \beta_c$ and in the limit $\Lambda \rightarrow \infty$ the solution satisfies $p^* \rightarrow -|h|$ thus validating (32).

5. Canonical analysis

The above analysis proves the existence of the transition and its unique properties. To get deeper understanding of the mechanism of the condensation transition it is instructive to study the model within the canonical ensemble. Critical phenomena are commonly described by Landau theory of phase transitions, which provides more details on the nature of such transitions. While the Landau theory is usually based on phenomenological analysis, in our case the model can be solved exactly and hence we can calculate the large deviation functions (LDF) F_M and F_N and their finite size corrections, which play the role of Landau free energy in this analysis. It turns out that unlike the basic assumption of the Landau theory, namely that the free energy is an analytic function of the order parameter, the functions F_M and F_N turns out to be non-analytic in n and m respectively.

5.1. Large deviations functions

To find the LDF and their finite size correction at zero external field we invert the z -transform (25) using the Cauchy integral formula, and use complex analysis techniques to evaluate the result to relevant order.

5.1.1. Magnetization large deviations function F_M For ease of notations we define

$$L_{\pm} \equiv \frac{1}{2}(L \pm M) \quad ; \quad z_{\pm} \equiv e^{\beta(p \pm h)} \quad ; \quad A \equiv e^{-\beta\Delta}. \quad (41)$$

We carry out the analysis for $M \geq 0$ (or $L_+ \geq L_-$). The LDF for $M < 0$ is obtained from that of $M > 0$ by symmetry. The partition function Z_M for the ensemble in which L and M (but not N) are fixed is given then by

$$Z_M(L, M; \beta) = \oint_{C_+} \frac{dz_+}{2\pi i} \oint_{C_-} \frac{dz_-}{2\pi i} \frac{\tilde{Q}(z_+, z_-; \beta)}{z_+^{L_++1} z_-^{L_-+1}}, \quad (42)$$

$$\tilde{Q}(z_+, z_-; \beta) \equiv Q\left(\frac{1}{\beta} \log(z_+ z_-), \frac{1}{\beta} \log(z_+/z_-), 0; \beta\right). \quad (43)$$

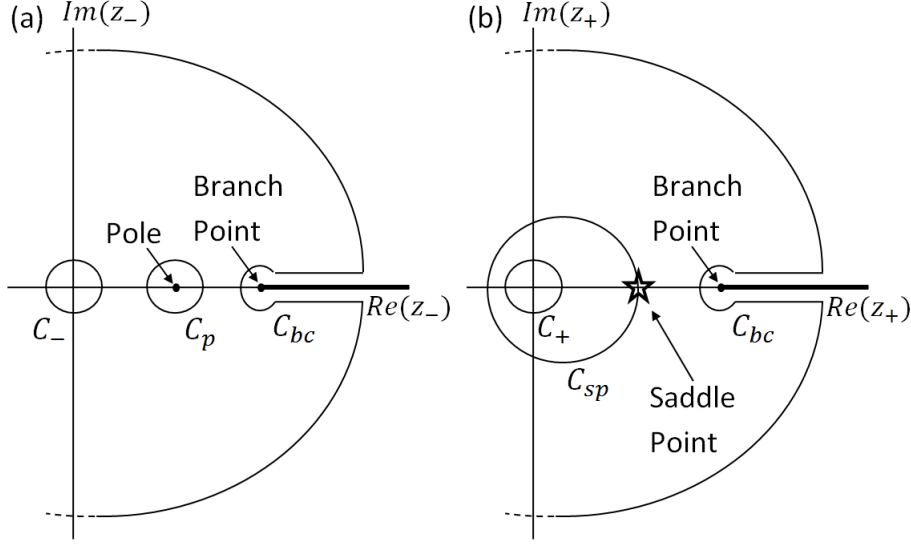


Figure 9. Contours of integration used in the calculations of Z_M and Z_N (see text).

Using the explicit form of Q (27) we get

$$Z_M(L, M; \beta) = \frac{A}{(2\pi i)^2} \oint \frac{dz_+ dz_-}{z_+^{L_++1} z_-^{L_-+1}} \frac{\Phi_{\beta C}(z_+) \Phi_{\beta C}(z_-)}{1 - A^2 \Phi_{\beta C}(z_+) \Phi_{\beta C}(z_-)}.$$

Carrying out the integration over z_- we note that for high enough temperatures the singularity closest to the origin in the z_- plane is a simple pole at $z_-^*(z_+)$ which satisfies

$$\Phi_{\beta C}(z_+) \Phi_{\beta C}(z_-^*) = A^{-2}. \quad (44)$$

This is the same equation as (31). Hence the contour of integration C_- can be deformed to a contour encircling this pole C_p , plus a contour with a larger radius C_{bc} (see Fig.9a). Due to the $z_-^{L_-}$ factor only the pole contour contributes, and hence

$$\begin{aligned} Z_M(L, M; \beta) &\approx \frac{1}{2\pi i A^3} \oint_{C_+} \frac{dz_+}{z_+^{L_++1}} \frac{(z_-^*)^{-L_-}}{\Phi_{\beta C-1}(z_+) \Phi_{\beta C}(z_-^*)} \\ &\equiv \frac{1}{2\pi i A^3} \oint dz_+ e^{-L f_m(m, z_+; \beta)}, \end{aligned} \quad (45)$$

$$f_m(m, z_+; \beta) = \left(\frac{1+m}{2} \right) \log[z_+] + \left(\frac{1-m}{2} \right) \log[z_-^*] + O\left(\frac{1}{L}\right). \quad (46)$$

We now proceed to carry out the integration over z_+ . In the z_+ plane there is a branch-cut for $z_+ \in [1, \infty)$ due to the polylogarithm function. If $f_m(m, z_+; \beta)$ has an extremum for $|z_+| < 1$, the saddle point method can be applied by deforming the contour C_+ to a contour C_{sp} which passes through the saddle point as in Fig.9b, yielding

$$F_M(m; \beta) = - \lim_{L \rightarrow \infty} \frac{1}{L} \log Z_M(L, M; \beta) = f_m(m, z_+^*(m; \beta); \beta), \quad (47)$$

with the saddle point z_+^* satisfying

$$0 = \frac{d}{dz_+} f_m(m, z_+; \beta)|_{z_+^*} = \frac{1+m}{2z_+^*} + \left(\frac{1-m}{2z_-^*} \right) \frac{dz_-^*}{dz_+} \Big|_{z_+^*}. \quad (48)$$

Eq.(47) is the result for the LDF F_M in the high temperature regime. We shall now show that at a certain temperature there is no longer a saddle point for $|z_+| < 1$ and hence a different approach should be followed. By differentiating Eq.(44) with respect to z_+ and using Eq.(48) the saddle point condition reads

$$\frac{\Phi_{\beta C-1}(z_+^*) \Phi_{\beta C}(z_-^*)}{\Phi_{\beta C}(z_+^*) \Phi_{\beta C-1}(z_-^*)} = \frac{1+m}{1-m}. \quad (49)$$

For fixed z_\pm^* the LHS of (49) is a decreasing function of β , while for fixed β it is an increasing function of z_+ as proved in Appendix A. The RHS of (49) is an increasing function of m , and hence $z_+^*(m; \beta)$ is an increasing function of both β and m . Therefore, for a given β such that $\beta C > 2$ there is a critical value of m , denoted m_c , such that for $m > m_c$ there is no saddle point for $|z_+| < 1$. The value of m_c is given by

$$\frac{\zeta(\beta C - 1) \Phi_{\beta C}(z_-^*(1))}{\zeta(\beta C) \Phi_{\beta C-1}(z_-^*(1))} = \frac{1+m_c}{1-m_c}. \quad (50)$$

If there is no saddle point, one can instead deform the contour C_+ to contour C_{bc} which wraps the branch cut and close in a large circle with radius tending to infinity as in Fig.9. The details of the calculations are involved and hence they are deferred to Appendix B. However the result is simple, namely z_+ is frozen at $z_+ = 1$ for all $m > m_c$, i.e.

$$F_M(m; \beta) = f_m(m, 1; \beta) = \left(\frac{1-m}{2} \right) \log [z_-^*(1)]. \quad (51)$$

Note that the analysis is valid for $m \geq 0$. For $m < 0$ the roles of z_+ and z_- should be inverted. Hence we find that for $m > m_c$ the LDF is linear in m as depicted in Fig.6a. From Eq.(44) it can be seen that $z_-^*(1)$ is an increasing function of β , which implies that the slope of m decreases with β (as $z_-^* < 1$). At some critical value β_c , one has $z_-^* = 1$ and thus F_M becomes flat (with 0 slope), as this is also the point where $m_c = 0$. The critical temperature is given by

$$\zeta(\beta_c C) = e^{\beta_c \Delta}, \quad (52)$$

which is the same as Eq.(35) for $h = 0$. For $\beta > \beta_c$ the singularity closest to the origin is no longer the pole (44) but the branch-point, and hence $F_M = 0$ for all m .

In summary the free energy $F_M(m; \beta)$ is given by (47) for $|m| < m_c$, and by (51) for $|m| > m_c$, with m_c given by (50) (see Fig.6a). The free energy is linear in m for $|m| > m_c$. Note that Eq.(44) defines implicitly the function $W_-(z_+, \beta)$ which appears in Eq.(18). Similarly $W_+(m, \beta)$ is defined implicitly by Eq.(49) for $|m| < m_c$ and by $z_+ = 1$ for $|m| \geq m_c$.

The linearity of the LDF for $|m| > m_c$ is a manifestation of a phase coexistence, i.e. it is the Maxwell construction [37]. The coexistence is between a normal phase which consists of microscopic domains and a phase with a single macroscopic domain. That is, the most probable way to implement a high magnetization $m > m_c$ is by breaking the system to a “normal gas” of domains with total density m_c and a macroscopic condensate with total density $m - m_c$. At the transition the slope of F_M

vanishes, which implies that the gas phase and the condensate phase have the same free energy (in the thermodynamic limit). This description may correspond just as well to a usual first order phase transition, and hence from this analysis it is not clear where does the mixed nature of the transition comes from. As we shall see in section 5.2, this comes from the logarithmic barriers in L between the phases.

5.1.2. Domains density large deviations function F_N The analysis for F_N is similar to the analysis of F_M , so some details will be spared. We start with

$$Z_N(L, N; \beta) = \frac{A}{(2\pi i)^2} \oint \frac{dz dq}{z^{L+1} q^{N+1}} \frac{q^2 \Phi_{\beta C}(z)^2}{1 - A^2 q^2 \Phi_{\beta C}(z)^2},$$

where $z = e^{\beta p}$ and $q = e^{\beta \mu}$. The pole equation which corresponds to the integration over q is

$$q^*(z; \beta) = \frac{1}{A \Phi_{\beta C}(z)}. \quad (53)$$

Again it is a special case of (31) for $h = 0$. Carrying out the pole integral yields

$$\begin{aligned} Z_N(L, N; \beta) &= \oint \frac{dz}{2\pi i} \frac{[A \Phi_{\beta C}(z)]^{L_N}}{A z^{L+1}} \\ &\approx \oint \frac{dz}{2\pi i} e^{-L f_n(n, z; \beta)}, \end{aligned} \quad (54)$$

$$f_n(n, z; \beta) \equiv \log z - n \log [A \Phi_{\beta C}(z)]. \quad (55)$$

A saddle point of f_n , when exists, is given by

$$\frac{\Phi_{\beta C-1}(z^*)}{\Phi_{\beta C}(z^*)} = \frac{1}{n}. \quad (56)$$

Deforming the contour to pass through it yields

$$F_N(n; \beta) = - \lim_{L \rightarrow \infty} \frac{1}{L} \log Z_N(L, N; \beta) = f_n(n, z^*; \beta). \quad (57)$$

The LHS of (56) is a decreasing function of β and an increasing function of z , while the RHS is a decreasing function of n , and therefore $z^*(n, \beta)$ is an increasing function of both β and n . Hence, if $\beta C > 2$ there exists n_c such that for $n < n_c$ there is no saddle point for $|z| < 1$, and n_c is given by

$$n_c = \frac{\zeta(\beta C)}{\zeta(\beta C - 1)}. \quad (58)$$

Then, by branch-cut integration (Appendix C) we get

$$F_N(n < n_c; \beta) = f_n(n, 1; \beta) = -n \log [A \zeta(\beta C)], \quad (59)$$

which is a linear function of n . This linearity is again a manifestation of the same coexistence between normal gas of microscopic domains (with domains density $n = n_c$) and a single macroscopic domain (with $n = \frac{1}{L} \rightarrow 0$). The analysis is valid both above and below β_c . For high temperatures ($\beta < \beta_c$) the slope is negative (as $\zeta(\beta C)$ is a decreasing function of β) and hence $n = 0$ is disfavored. At the critical temperature $A(\beta_c) \zeta(\beta_c C) = 1$ by Eq.(52). Hence $F_N(n < n_c) = 0$, implying coexistence between the gas ($n = n_c$) and the condensate ($n = 0$) in the unconstrained system. For $\beta > \beta_c$ the slope is positive which implies that the thermodynamically stable phase is one with $n = 0$.

For $\beta C \leq 2$ one has $n_c = 0$. From (56-57) it can be deduced that n^* , the minimum of F_N , is a decreasing function of temperature. If $c \equiv \beta_c C \leq 2$ it implies that $n \rightarrow 0$ in a continuous manner as $\beta \rightarrow \beta_c$. On the other hand, if $c > 2$ then at high temperatures there is no linearity (no coexistence with a condensate phase) but at temperatures $\beta = 2/C < \beta_c$ a coexistence initiates for small n or for large m .

In summary the free energy $F_N(n; \beta)$ is given by Eqs.(55-57) for $n > n_c$, and is a linear function given by Eq.(59) for $n < n_c$, where n_c is given by Eq.(58). For $c \leq 2$, $n_c = 0$ and hence there is no linear part. The function $W_n(n, \beta)$ appearing in Eq.(21) is defined by Eq.(56) for $n > n_c$ and by $z^* = 1$ for $n \leq n_c$.

5.2. Finite size corrections

The above analysis establishes the fact that m is discontinuous at the transition for all $c \equiv \beta_c C > 1$. Moreover, while n is discontinuous for $c > 2$, it is continuous for $c \leq 2$. The canonical analysis presents a scenario which seems like a conventional first order transition. But as discussed above, even though the order parameter is discontinuous, at the transition there are features of a critical transition such as divergence of correlation length and diverging susceptibility (for $c < 3$). How can this be explained in the framework of the canonical analysis, i.e. as an outcome of the form of the “Landau free energy”? This question is answered by looking into the finite size corrections to the large deviations functions, which turn up to be logarithmic in L as we shall show below. These logarithmic barriers can be understood as the usual surface energy between coexisting phases that appears in first order transitions. In d -dimensional models with short range interactions the surface energy scales like L^{d-1} , hence at $d = 1$ it is of order $O(1)$ or $O(\log(L))$. However this is a somewhat simplistic argument since in this case the logarithmic scaling relies also on the effective r^{-2} interaction between spins. Below we shall derive the finite size correction for Z_N and Z_M and show that at and below the critical temperature there are logarithmic barriers.

5.2.1. Corrections to Z_N To go beyond the LDF result (57) when a saddle point exists, i.e. for $n > n_c$, we note that the saddle point method yields a sub-leading term due to the second derivative of the integrand, i.e.

$$Z_N(L, Ln; \beta) \approx \sqrt{\frac{2\pi}{L |\partial_z^2 f_n(n, z^*; \beta)|}} \frac{[A\Phi_{\beta C}(z^*)]^{Ln}}{Az^{*L+1}}.$$

Calculating explicitly $\partial_z^2 f_n$ yields

$$Z_N(L, Ln; \beta) \approx \left[2\pi L \left| \frac{1}{z^{*2}n} - \frac{\Phi''_{\beta C}(z^*)}{\Phi_{\beta C}(z^*)} n \right| \right]^{-\frac{1}{2}} \frac{[A\Phi_{\beta C}(z^*)]^{Ln}}{Az^{*L+1}}. \quad (60)$$

This implies that the correction to the extensive free energy is logarithmic as stated above. For $n < n_c$ the correction comes from the explicit result for the branch-cut integration (see Eq.(96)), i.e.

$$Z_N(L, Ln; \beta) \approx \frac{b_\phi(n)\Gamma(\beta C)}{\pi L^{\beta C-1} (b_\Lambda(n))^{\beta C-2}} [A\zeta(\beta C)]^{Ln}, \quad (61)$$

(Λ here is not the same as the one define in section 4.3) with

$$b_\Lambda(n) = 1 - \frac{n\zeta(\beta C - 1)}{\zeta(\beta C)},$$

$$b_\phi(n) = n \frac{\pi}{\Gamma(\beta C) \zeta(\beta C)}.$$

For $n = n_c = \zeta(\beta C) / \zeta(\beta C - 1)$ (Eq.(58)), $b_\Lambda(n_c) = 0$ and hence the approximation breaks down near $n = n_c$. The breakdown of the branch cut integration approximation is due to the proximity of the branch point and pole when $n \approx n_c$. Calculating the finite size corrections for $n \approx n_c$ requires a different approach, which will not be discussed here.

The free energy resulting from the approximation of Eqs.(60-61) with $L = 1000$ is plotted in Fig.7a, together with an exact evaluation of the partition function for the same value of L . The exact evaluation was done numerically as described in Appendix D. Comparing the approximation and the exact evaluation it can be seen that the approximations are quite accurate, except around $n = n_c$. At the critical point, i.e. when $z^* = 1$ and $A\zeta(\beta_c C) = 1$, Z_N contain only powers of L and no exponential (or stretched exponential) terms. This indicates that fluctuations of n would be distributed asymptotically as a power law and hence that the transition will be scale invariant. Together with the discontinuity in n (for $c > 2$) this implies that the transition is MOT.

To verify that the free energy barriers are logarithmic (corresponding to power law dependence of Z_N in L) we define R as in (22) to be the integral of $\tilde{F}_N = -\frac{1}{L} \log Z_N(L, N)$ from $n = 0$ to the minimum of \tilde{F}_N at n^* . From Eqs.(60-61) it can be seen that \tilde{F}_N has a single minimum at $n^* > n_c$ and hence R is well defined. We then evaluate R numerically and plot it in Fig.8. From this figure it is apparent that R scales logarithmically. This confirms that any free energy barrier between 0 and n^* is logarithmic in L .

5.2.2. Corrections to Z_M Following similar steps as in the previous section we can find the finite size corrections for Z_M , but in this case the approximation fails near the critical temperature and below it because Eq.(44) has no solution. Hence instead we shall use a simple argument to obtain the leading order finite size behavior of Z_M well below the critical temperature. Specifically, in the regime where the gas phase is unstable, we can expect that any magnetization is realized (to leading order) by a phase separation of the chain to a + condensate and a - condensate, their lengths are set by the condition that the given magnetization is realized. This simply implies

$$Z_M(L, m; \beta > \beta_c) \sim \left(\frac{1+m}{2} L \right)^{-\beta C} \left(\frac{1-m}{2} L \right)^{-\beta C}. \quad (62)$$

This approximation is plotted in Fig.7b along with the exact numerical evaluation of the free energy (see Appendix D) for $L = 1000$, and seems to fit very well. Here again we see that there are no exponential terms, and magnetization fluctuations are suppressed only in a power law manner and not exponentially.

6. RG analysis

As was shown above, many features of the model can be obtained analytically in more than one way. However, the main tool used to study the IDSI model and related models was the renormalization group (RG) analysis [23, 6]. To study the relation of our model to those models we shall carry out an (approximate) RG analysis to our model and compare it to the RG of the IDSI model, stressing the similarities and differences.

6.1. Model definition

For the scaling — or renormalization group (RG) — analysis, it is useful to define an off-lattice version of the model (7). This version also makes the connection to coulomb gas models and the Kosterlitz-Thouless scenario more explicit.

We consider a gas of N particles on an interval $[0, L]$, or on the circle if periodic boundary conditions are considered. The particles represent the domain boundaries (kinks) of the lattice version, and following (7), each pair of nearest neighboring particles interact through an attractive logarithmic potential. To avoid divergences there is an ultraviolet cutoff scale a which is the hard-core of the particles, so that the Hamiltonian takes the form

$$H(\{r_i\}; N) = C \sum_{i=1}^N \log \left(\frac{r_{i+1} - r_i}{a} \right) + N\Delta \quad \text{with } |r_{i+1} - r_i| \geq a$$

This constitutes the Coulomb gas picture of the model.

6.2. RG analysis

The grand canonical partition function takes the form

$$Z_C(L; A, K) = \sum_{N=1}^{\infty} A^N \int_{-\infty}^{\infty} \frac{dr_1}{a} \int_{-\infty}^{\infty} \frac{dr_2}{a} \dots \int_{-\infty}^{\infty} \frac{dr_N}{a} \prod_{i=1}^N \left(\frac{r_{i+1} - r_i}{a} \right)^{-K} \Theta(r_{i+1} - r_i - a), \quad (63)$$

where $A \equiv e^{-\beta\Delta}$ and $K = \beta C$. This integral can be calculated exactly, as we have done above, but here we shall follow the RG protocol of [6]: First we rescale the core-size $a \rightarrow ae^\kappa$ for $0 < \kappa \ll 1$. Then we express the partition sum in terms of rescaled parameters A_κ and K_κ such that in terms of these parameters it has the same form as the original partition sum. This implies

$$Z_C(L; A, K) = \sum_{N=1}^{\infty} A_\kappa^N e^{N\kappa(K_\kappa-1)} \int_{-\infty}^{\infty} \dots \int_{-\infty}^{\infty} \prod_{i=1}^N \frac{dr_i}{a} \left(\frac{r_{i+1} - r_i}{a} \right)^{-K_\kappa} \Theta(r_{i+1} - r_i - ae^\kappa).$$

Applying the expansion

$$\Theta(r_{i+1} - r_i - ae^\kappa) = \Theta(r_{i+1} - r_i - a) - a\kappa\delta(r_{i+1} - r_i - a) + O(\kappa^2),$$

we get to first order in κ

$$\begin{aligned} Z_C(L; A, K) &= Z_C\left(L; A_\kappa e^{\kappa(K_\kappa-1)}, K_\kappa\right) \\ &\quad - a\kappa \sum_{N=1}^{\infty} A_\kappa^N \sum_j \int_{-\infty}^{\infty} \prod_{i \neq j, j-1} \left[\frac{dr_i}{a} \left(\frac{r_{i+1} - r_i}{a} \right)^{-K_\kappa} \Theta(r_{i+1} - r_i - a) \right] dr_{j-1} \times \\ &\quad \int_{r_{j-1}+a}^{r_{j+1}-a} \left(\frac{r_{j+1} - r_j}{a} \right)^{-K_\kappa} \left(\frac{r_j - r_{j-1}}{a} \right)^{-K_\kappa} dr_j \delta(r_{j+1} - r_j - a), \end{aligned} \quad (64)$$

The integral in the last line of (64) results in

$$\left(\frac{r_{j+1} - r_{j-1} - a}{a} \right)^{-K} \Theta(r_{j+1} - r_{j-1} - 2a).$$

Up to this point the calculation is exact, but here we should introduce a physical argument which enables one to write closed RG equations. The physical picture is of kinks interacting in nearest-neighbor pairs. If the density of kinks is small (i.e.

$A \ll a^{-1}$) it implies that the typical distance between a pair is large and hence it is plausible to assume $r_{j+1} - r_{j-1} - a \approx r_{j+1} - r_{j-1}$. Therefore the result (to first order in κ) is

$$Z_C(L; A, K) = \sum_{N=1}^{\infty} A_{\kappa}^N \left(e^{N\kappa(K_{\kappa}-1)} - a\kappa N A_{\kappa} \right) \times \\ \int_{-\infty}^{\infty} \dots \int_{-\infty}^{\infty} \prod_{i=1}^N \frac{dr_i}{a} \left(\frac{r_{i+1} - r_i}{a} \right)^{-K_{\kappa}} \Theta(r_{i+1} - r_i - a).$$

To compensate for the additional factor $(e^{N\kappa(K_{\kappa}-1)} - a\kappa N A_{\kappa})$ such that the partition sum retains its original form, the renormalized parameters A_{κ} and K_{κ} are taken to be in leading order in κ

$$A_{\kappa} = A(1 + \kappa(1 - K + aA)) + O(\kappa^2), \\ K_{\kappa} = K + O(\kappa^2).$$

Defining $x \equiv 1 - K$ and $y \equiv aA$ the resulting flow equations are

$$\frac{dy}{d\kappa} = xy + y^2, \quad (65)$$

$$\frac{dx}{d\kappa} = 0. \quad (66)$$

The physical intuition behind these flow equations is the following: A change of scale has two effects. First, due to the change of scale the density — and hence the fugacity y — renormalizes. This is accounted by the first term of (65). Second, rescaling of the core size might cause near-by kinks to merge. The likelihood of having two adjacent kinks scales as y^2 , implying the second term. For far away (but nearest neighbors) kinks, the effect of two kinks that merged is the same as a single kink, as the interaction is anyway between nearest neighbors. Since these are the only outcomes of the scale transformation (to leading order), the interaction x is kept constant.

The RG flow diagram has a line of fixed points at $y = 0$ which are stable for $x < 0$ and are unstable for $x > 0$. It has another line of unstable fixed points at $y = -x$ for $x < 0$, which is the line of phase transition: flow lines which start above this line increase in y until the validity of the analysis breaks down (the condition $y \ll 1$ is no longer valid) and hence flow into the disordered phase, while flow lines which start below this line flow parallel to the y axis into the corresponding $y = 0$ fixed point, which is the ordered phase. The details of the flow diagram are presented in Fig.10a together with the exact phase transition line.

From the RG equations we can calculate the behavior of the correlation length near the transition. This is done by integrating the flow equations, starting just above the critical line $y^* = -x$, i.e. at $y = -x + \delta y$ with $\delta y \sim T - T_c$, and ending at $y = 1$, where the analysis breaks down but the correlations are order 1. Then Eq.(65) yields

$$d\kappa = \frac{dy}{xy + y^2} \Rightarrow \\ \kappa = \left[\frac{1}{x} \log \left(\frac{y}{x + y} \right) \right]_{-x+\delta y}^1.$$

Using $\xi \sim e^{\kappa}$ and $\delta y \sim T - T_c$, the leading order term is

$$\xi \sim \left(\frac{T - T_c}{|x|} \right)^{\frac{1}{x}}.$$

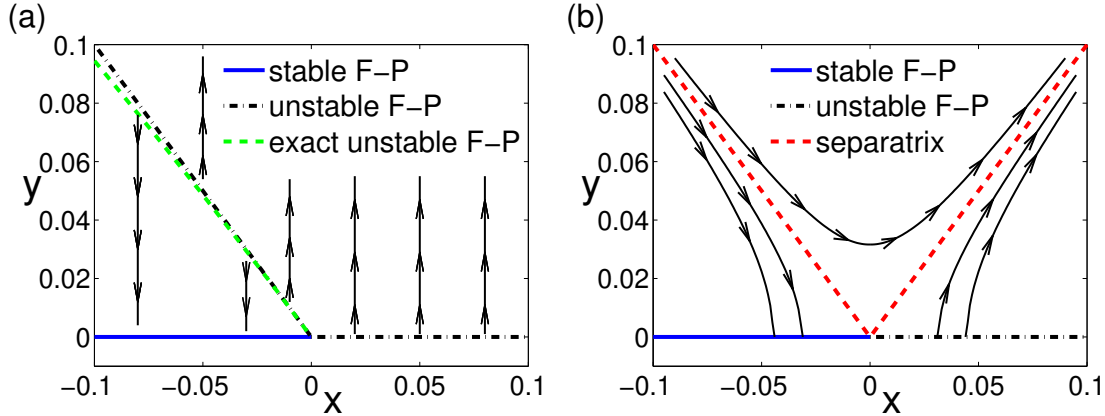


Figure 10. (color online) RG flow for (a) TIDSI model, Eqs.(65-66) and (b) IDSI model (or XY model), Eq.(67-68).

Using $x = 1 - \beta_c C$, this is the same as Eq.(15). The exponent $1/x$ diverges for $x \rightarrow 0_-$ suggesting that in this limit an essential singularity develops.

6.3. Comparison with the flow diagram of IDSI and related models

The IDSI model, like other models with r^{-2} interactions, has a very similar representation as an interacting gas of charges [6]. The only difference between TIDSI model and the IDSI model is that in the IDSI all the charges interact with each other logarithmically, while in the TIDSI model the interactions are only between nearest neighbors. This implies that in the IDSI model, when two opposite charges are close by they screen the effect of each other, and therefore to leading order they cancel out and they contribute only a dipole moment. This dipole moment turns out to renormalize the logarithmic interaction between other charges, exactly in the same manner that the screening of close by vortices renormalizes the interactions between vortices in the XY model. Hence the y^2 term in (65), which appears due to merging of two charges, is transferred to the flow equation for x and the resulting flow equations for the IDSI model read

$$\frac{dy}{d\kappa} = xy, \quad (67)$$

$$\frac{dx}{d\kappa} = y^2, \quad (68)$$

where x and y are defined essentially the same as above. This flow has only one line of fixed points at $y = 0$, but it also has a separatrix at $y = |x|$. The phase transition is along the line $y = -x$ for $x < 0$, where flow lines starting below it flow to the $y = 0$ fixed line (ordered phase) while flow lines that start above it flow to the disordered phase, but the transition is controlled by a single critical point $x = y = 0$. The flow in the IDSI and TIDSI case can be compared in Fig.10. A consequence of the different flow equations is the behavior of the correlation length, which diverges algebraically in the TIDSI model while it exhibits an essential singularity for the IDSI model. This is an outcome of the flow near the critical point (or critical line in the case of the TIDSI model): while linearizing Eq.(65-66) near $y = -x$ line we find that the flow is linear

in the TIDSI model, the flow is obviously quadratic in the IDSI case. This difference yields the different behavior of the correlation length.

It is interesting to note that the lack of renormalization of the coupling constant x appears also in the context of discrete Gaussian chain [8]

$$H = - \sum_{ij} J_{ij} (h_i - h_j)^2 \quad ; \quad J_{ij} \sim |i - j|^{-2},$$

where the height variables h_i are integers, and with the boundary condition $h_0 = 0$. This problem can also be mapped onto a dissipative quantum particle in a periodic potential [38]. In this case there are infinitely many fugacities y_k corresponding to kinks with $h_i - h_j = k$, all renormalize due to both the density scaling and merging of kinks, but the coupling coefficient does not rescale. The connection between the TIDSI model and the discrete Gaussian chain can be a subject of future investigations.

7. Generalizations

The TIDSI model can be generalized without losing its solubility. Below we first generalize the decay of interactions between spins beyond the inverse square law of $J(r)$ in (4). We then consider the inverse squared law but with spin models other than spin $\frac{1}{2}$ Ising model, namely Potts model and general Ising model.

7.1. General interactions decay law

7.1.1. Definition In this section we consider the Hamiltonian (4) with

$$J(r) = Cr^{-\alpha}, \quad (69)$$

where $\alpha > 1$. The long-range self energy of a domain H_{LR} can be estimated as before to be

$$H_{LR}(l) = -C \sum_{k=1}^l \frac{l-k}{k^\alpha} = -C\zeta(\alpha)l + C \left(\frac{1}{\alpha-1} + \frac{1}{\alpha-2} \right) l^{2-\alpha} + O(1). \quad (70)$$

As before, the linear term will contribute a constant in the total energy. For $\alpha > 2$ the subleading term is $O(1)$, and hence there is no transition. We thus restrict the discussion in this paper to $1 < \alpha < 2$. After readjusting the ground state energy, the Hamiltonian reads

$$H^{(\alpha)}(\{l_a\}; N) = C_\alpha \sum_{a=1}^N l_a^{2-\alpha} + \Delta N, \quad (71)$$

with $C_\alpha \equiv C \left(\frac{1}{\alpha-1} + \frac{1}{\alpha-2} \right)$ and $\Delta = 2J_{NN}$.

7.1.2. Analysis The analysis of the above model in the grand canonical ensemble is very similar to the one done in section 4. Skipping some details, the generating function is now

$$Q(p, h, \mu; \beta) = \frac{e^{2\beta(\mu-\Delta)} W_\alpha(p+h) W_\alpha(p-h)}{1 - e^{2\beta(\mu-\Delta)} W_\alpha(p+h) W_\alpha(p-h)}, \quad (72)$$

with

$$W_\alpha(x) = \sum_l \exp(\beta x l - \beta C_\alpha l^{2-\alpha}) \equiv \Psi_{\beta C_\alpha}^\alpha(e^{\beta x}). \quad (73)$$

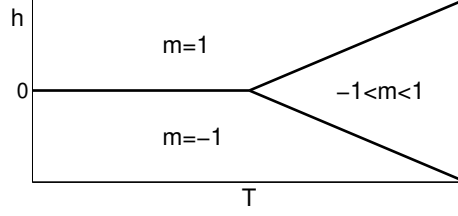


Figure 11. Schematic phase diagram for model (71).

Note that the functions W_α and $\Psi_{\beta C}^\alpha$ have nothing to do with the functions $W_\pm()$, $W_n()$ and $\Psi_\pm()$ defined in previous sections. The relevant properties of $\Psi_\gamma^\alpha(u)$ for $1 < \alpha < 2$ are:

- (i) $\Psi_\gamma^\alpha(u)$ is analytic in the complex plane except for a branch-cut along $[1, \infty)$
- (ii) $\frac{d^n}{du^n} \Psi_\gamma^\alpha(u)|_{u=1} < \infty$ for any $n \geq 0$.

Due to the similarity between the properties of $\Psi_\gamma^\alpha(u)$ and those of the polylogarithm function $\Phi_\gamma(u)$, the analysis of this case is very similar to the one done for the $\alpha = 2$ case. Hence the analysis done above for the case $\alpha = 2$ holds also for this case. The critical temperature for $\mu = 0$ and $h \geq 0$ is given by

$$\Psi_{\beta C_\alpha}^\alpha(1) \Psi_{\beta C_\alpha}^\alpha(e^{\beta(p-h)}) = e^{2\beta\Delta},$$

and specifically for $h = 0$ it is

$$e^{\beta\Delta} = \Psi_{\beta C_\alpha}^\alpha(1) \equiv \sum_l \exp(-\beta C_\alpha l^{2-\alpha}).$$

Due to the finiteness of the derivatives of Ψ_γ^α , the transition is discontinuous (both in m and n) for any value of C_α and h . A schematic phase diagram is depicted in Fig.11. The $h = 0$ transition line between the two magnetically saturated phases is an ordinary first order phase transition, while the two transition lines separating the magnetically unsaturated phase from the saturated ones are MOT, like in the $\alpha = 2$ case. However, unlike the latter case, the distribution of domain sizes is not power law even at the transition, and instead it takes a form similar to Eq.(38)

$$P_\pm(l) \simeq e^{\beta(p^* \pm h)l} e^{-\beta C_\alpha l^{2-\alpha}} \equiv \exp \left[-\frac{l}{\xi_\pm} - \left(\frac{l}{\xi_\alpha} \right)^{2-\alpha} \right]. \quad (74)$$

The exponential length scales ξ_\pm diverges at the transition just like in the $\alpha = 2$ case and hence the transition is MOT. However, at the transition $P_\pm(l)$ takes a stretched exponential form and hence all its moments are finite, unlike in that case. The stretched exponential law defines a different length scale $\xi_\alpha \equiv (\beta C_\alpha)^{\frac{1}{2-\alpha}}$, which sets the scale of correlations. It can be seen that indeed this length scale diverges for $\alpha = 2$ and $\beta C_\alpha > 1$.

7.2. General spins

We return now to $J(r) \approx Cr^{-2}$ case, but consider more general spin models. For concreteness, we focus on Potts spins and general Ising spins, but other models can be analyzed following the same steps. Specifically, we show that such models can be solved exactly using the transfer matrix approach.

7.2.1. Potts spins We consider now a chain of L spins σ_i that can take a value in $[1..K]$ with a Hamiltonian analogous to Eq.(4), i.e.

$$H = -J_{NN} \sum \delta_{\sigma_i, \sigma_{i+1}} - \sum_{i < j} J(i-j) \delta_{\sigma_i \sigma_j} I(i \sim j). \quad (75)$$

Due to the truncation of the LR interactions the term $\delta_{\sigma_i \sigma_j}$ within each domain is always unity. The model can be casted in the domains representation, in which a configuration is composed of N domains with sizes $\{l_n\}$ and spins $\{s_n\}$. A domain self energy then has a very similar form to Eqs.(5,6), which yields the same Hamiltonian as (7), i.e.

$$H(\{l_n\}, \{s_n\}; N) = C \sum_{n=1}^N \log(l_n) + \Delta N + Const. \quad (76)$$

As there are K symmetric spin states in this case and not only two, a natural ensemble to consider is one where the set $\{L_s\}_{s=1}^K$ is fixed, where L_s is the total number of spins of type s . The partition function of such an ensemble, where in addition N is fixed, is

$$Z_0(\{L_s\}, N; \beta) = \sum_N \sum_{\{l_n\}} \sum_{\{s_n\}} \prod_{n=1}^N \frac{e^{-\beta \Delta}}{l_n^{\beta C}} I(s_n \neq s_{n-1}) \prod_{s=1}^K I\left(\sum l_n \delta_{s_n, s} = L_s\right).$$

A set of K order parameters can be constructed as

$$m_s = \frac{KL_s - L}{L(K-1)}. \quad (77)$$

To define the corresponding grand partition function we should therefore introduce $K+1$ fugacities (μ and p_s , $s = 1..K$) corresponding to the $K+1$ constraints (fixed N and $\{L_s\}$). Then the grand partition function is

$$Q(p, h, \mu; \beta) = \sum_N \prod_{n=1}^N e^{\beta(\mu - \Delta)} \sum_{s_n \neq s_{n-1}} U_{\beta C}(p_{s_n}), \quad (78)$$

$$U_\rho(x) \equiv \sum_l \frac{e^{\beta x l}}{l^\rho}. \quad (79)$$

To proceed we define the transfer matrix,

$$\hat{T}_{\sigma\tau} = \begin{cases} e^{\beta(\mu - \Delta)} U_{\beta C}(\beta p_\tau) & \sigma \neq \tau \\ 0 & \sigma = \tau \end{cases}. \quad (80)$$

Assuming for simplicity fixed boundary conditions s_1 and s_N , and using conventional bra-ket notations, the grand-partition function can be expressed as

$$\begin{aligned} Q(\{p_s\}, \mu; \beta) &= \sum_{N=1}^{\infty} \langle s_1 | \hat{T}^N | s_N \rangle \\ &= \langle s_1 | \frac{\hat{T}}{1 - \hat{T}} | s_N \rangle. \end{aligned} \quad (81)$$

We can first set $\mu = 0$ and $p_s = p$ for all s , i.e. constraining only the total size L . As before, the most negative singularity of Q in p can stem either from the denominator, where the maximal eigenvalue of the matrix $\hat{T}(p)$ satisfies $\lambda_{max} = 1$, i.e.

$$p^* = \arg \min_p \{ \lambda_{max}(p) = 1 \}, \quad (82)$$

or from the branch point of $U_{\beta C}$, at

$$p^* = 0. \quad (83)$$

In this setting the eigenvalues of \hat{T} can be obtained exactly, and the maximal eigenvalue is

$$\lambda_{max} = (K - 1) e^{-\beta \Delta} U_{\beta C}(p).$$

Hence for low enough temperature, $p^* = 0$, which as in the TIDSI implies a condensation transition.

To see that indeed there is condensation, we can set $p_1 = p + r$ and $p_s = p$ for all $s > 1$. Then

$$\frac{L_1}{L} = - \left. \frac{dp^*}{dr} \right|_{r=0}.$$

The largest eigenvalue of \hat{T} is given by

$$\lambda_{max} = \frac{e^{-\beta \Delta}}{2} \left[(K - 2) U_{\beta C}(p) + \sqrt{(K - 2)^2 U_{\beta C}(p)^2 + (4K - 4) U_{\beta C}(p) U_{\beta C}(p + r)} \right].$$

Hence in the high temperature phase, for which p^* is set by the condition $\lambda_{max} = 1$, we find by straightforward calculation

$$L_1 = \frac{L}{K} \quad \Rightarrow \quad m_1 = 0,$$

while in the low temperature phase $p^* = -r$ (for $r > 0$) and therefore

$$L_1 = L \quad \Rightarrow \quad m_1 = 1.$$

This implies that the order parameter m_1 jumps from 0 to 1 at the transition just like in the original TIDSI. Finally the domain size distribution (at $r = 0$) can be written, in analogy with Eq.(38), as

$$P(l) \simeq \frac{Z_C(L - l, h)}{Z_C(L, h)} \times \frac{1}{l^{\beta C}} = \frac{e^{-\beta p^* l}}{l^{\beta C}} = \frac{e^{-l/\xi}}{l^{\beta C}},$$

with $\xi = \log(p^*)^{-1}$ being the diverging length scale. Hence the transition is MOT of the same kind as in the original TIDSI.

7.2.2. General Ising spins Now we consider a spin $\frac{K}{2}$ Ising model, i.e. where each spin σ_i can take one of $K+1$ different values $\{-K, -K+2, \dots, K\}$. The Hamiltonian is

$$H = -J_{NN} \sum \sigma_i \sigma_{i+1} - \sum_{i < j} J(i - j) \sigma_i \sigma_j I(i \sim j). \quad (84)$$

Now, different domains have different energies according to their spin. The Hamiltonian in the domains variables read

$$H(\{l_n\}, \{s_n\}; N) = - \sum_{n=1}^N B_1 s_n^2 l_n + C \sum_{n=1}^N s_n^2 \log(l_n) + \sum_{n=1}^N (B_2 s_n^2 - J_{NN} s_n s_{n+1}) + Const,$$

where B_1 and B_2 are positive coefficients. The grand canonical partition function has the same form as in the Potts model, i.e. Eq.(81), with the transfer matrix

$$\hat{T}_{\sigma\tau} = \exp [\beta (\mu - B_2\tau^2 + J_{NN}\sigma\tau)] U_{\beta C\tau^2} (p_\tau + B_1\tau^2),$$

for $\sigma \neq \tau$ and $\hat{T}_{\sigma\sigma} = 0$. The function $U_\rho(x)$ is defined by Eq.(79). Setting $p_\tau = p$ and $\mu = 0$, the thermodynamic limit is obtained when either the maximal eigenvalue is unity, i.e.

$$\lambda_{max}(p^*) = 1, \quad (85)$$

or at

$$p^* = -\max_{\tau} \{B_1\tau^2\} = -B_1K^2. \quad (86)$$

Calculating λ_{max} is hard and does not provide any new insights. However as \hat{T} is a non-negative irreducible matrix, the Perron-Furbenius theorem implies that $\lambda_{max} > 0$. Moreover, for $J_{NN} < B/K$ increasing β decreases (or do not change) all the elements of \hat{T} , thus by Wielandt's theorem [39] λ_{max} also decreases with β . The reverse goes for increasing p , and hence in the high temperature phase, where p^* is set by Eq.(85), p^* is an increasing function of β . Therefore there is a critical β for which $\lambda_{max}(B_1K^2) = 1$, which sets the transition temperature. Adding to the Hamiltonian a magnetic field h which is coupled to the magnetization order parameter $m = \frac{1}{L} \sum l_n s_n$ amounts to setting $p_\tau = p + \tau h$. The maximal eigenvalue λ_{max} must be symmetric with respect to $h \rightarrow -h$, and hence in the high temperature regime $m = 0$. In the low temperature regime $p^* = -B_1K^2 - |h|K$ which implies that $m = \pm K$ as expected. Hence, while there is full magnetization also in this model, the spin of the macroscopic domain is only two fold degenerate, and not K (or $K + 1$) fold degenerate as in the Potts model case.

8. Conclusions

In this paper we present a detailed analysis of the TIDSI model which was recently introduced in [1]. The study is motivated by the observation that this is an exactly soluble model which exhibits a mixed order transition and which serves as a link between different classes of models exhibiting MOT. The steady state of the model and its phase diagram are first calculated in the grand canonical ensemble. In addition a canonical analysis which sheds new light on the mechanism of a mixed order transition is presented. This analysis shows that for $c > 2$, where both order parameters, the magnetization m and the domains density n , are discontinuous, criticality stems from logarithmic barriers in the effective Landau free energy. For $c < 2$ where n is continuous, the magnetization m remains discontinuous due to spin inversion symmetry in the high temperature phase. We also elaborate on the RG analysis presented in [1], and finally generalize the model by introducing general power-law decaying interactions ($1/r^\alpha$) and several other types of spin variables. These generalizations elucidate the special features of the borderline case $\alpha = 2$ and show that MOT can take place in a rather general class of discrete spin models.

The TIDSI model provides a bridge between one dimensional models with $1/r^2$ interactions such as the IDSI and one dimensional models exhibiting the depinning transition, like the PS model. This opens a window for a more general question regarding the connection between models exhibiting mixed order transitions. For instance, the spiral model of [14, 15] is a two dimensional model which exhibits MOT.

Can the mechanism which leads to the transition to the jammed state be related to that of the one dimensional models exhibiting MOT discussed in this paper? In the context of networks, there has been a recent debate [40, 41] regarding the nature of transition of a process dubbed “explosive percolation” in which an irreversible network evolution models exhibit a rather abrupt appearance of a giant component. There is some evidence [21, 20] that this process, or some version of it, leads to a mixed order transition, with a finite size behavior similar to TIDSI (i.e. logarithmic barriers). Can this process, and related percolation models like k -core percolation [17] be connected with our model? A general framework for studying such mixed order transitions is still missing.

Another interesting and not thoroughly explored direction of research has to do with the dynamics of (equilibrium) models exhibiting MOT. Phase separation kinetics is the dynamical behavior of systems quenched from a high temperature phase, usually infinite temperature, to a low temperature ordered phase. The phase ordering kinetics of systems exhibiting second order phase transitions, usually at zero temperature [42] has been a subject of a large body of work in recent years. However, it seems that there are no elaborate studies of the phase ordering kinetics in models exhibiting MOT. In [43] the phase ordering kinetics of the IDSI and other models with long-range interactions were studied, but only at zero temperature, while a more interesting case would be quenching to the critical temperature, in which unlike in second order transitions, real phase ordering is expected. Another intriguing question in this context is the connection of the dynamics of the TIDSI model with nonequilibrium models with absorbing states. This is left for future work.

We thank M. Aizenman, O. Cohen and O. Hirschberg for helpful discussions. The support of the Israel Science Foundation (ISF) and of the Minerva Foundation with funding from the Federal German Ministry for Education and Research is gratefully acknowledged. We also thank the Galileo Galilei Institute for Theoretical Physics for the hospitality and the INFN for partial support during the completion of this work.

A. Analysis of the LHS of Eq.(49)

We wish to show that

$$g(z_+) \equiv \frac{\Phi_{\beta C-1}(z_+) \Phi_{\beta C}(z_-^*(z_+))}{\Phi_{\beta C}(z_+) \Phi_{\beta C-1}(z_-^*(z_+))},$$

is an increasing function of z_+ for fixed β . The function z_-^* is given by the implicit relation (44), i.e.

$$\Phi_{\beta C}(z_-^*) = [A^2 \Phi_{\beta C}(z_+)]^{-1},$$

implying that z_-^* is a decreasing function of z_+ . The function g can be written as $g(z_+) = h(z_+)/h(z_-^*)$ where

$$h(u) \equiv \frac{\Phi_{\beta C-1}(u)}{\Phi_{\beta C}(u)}.$$

Showing that $h(u)$ is an increasing function thus proves that $g(z_+)$ is also an increasing function.

To show that h is increasing we inspect its derivative

$$\frac{dh(u)}{du} = \frac{\Phi_{\beta C-2}(u) \Phi_{\beta C}(u) - \Phi_{\beta C-1}(u)^2}{u \Phi_{\beta C}(u)^2} \equiv \frac{\mathcal{N}}{\mathcal{D}}.$$

The denominator \mathcal{D} is trivially positive and it is left to show the same for the numerator \mathcal{N} :

$$\begin{aligned}
\mathcal{N} &= \sum_{k,l=1}^{\infty} \left[\frac{u^l}{l^{c-2}} \frac{u^k}{k^c} - \frac{u^l}{l^{c-1}} \frac{u^k}{k^{c-1}} \right] \\
&= \sum_{k,l=1}^{\infty} \frac{u^l}{l^{c-1}} \frac{u^k}{k^c} [l - k] \\
&= \sum_{k < l}^{\infty} u^{l+k} [l - k] \left[\frac{1}{l^{c-1}} \frac{1}{k^c} - \frac{1}{k^{c-1}} \frac{1}{l^c} \right] \\
&= \sum_{k < l}^{\infty} \frac{u^{l+k}}{l^c k^c} [l - k]^2 > 0.
\end{aligned}$$

Q.E.D.

B. Approximating (45) without saddle point

Here we calculate the integral (45) when $f_m(m, z_+)$ has no saddle point for $|z_+| < 1$, i.e. in the regime $\beta < \beta_c$ and $m > m_c$, which implies $\beta C > 2$. In this case the contour of the integral can be deformed as presented in Fig.9b. The contour C_{bc} can be expressed as concatenation of four parts which are

$$\begin{aligned}
(I) &: [R - i\epsilon, 1 - i\epsilon], \\
(II) &: \left\{ 1 - \epsilon e^{i\theta} : \frac{\pi}{2} < \theta < \frac{3\pi}{2} \right\}, \\
(III) &: [1 + i\epsilon, R + i\epsilon], \\
(IV) &: \{ R e^{i\theta} : \delta < \theta < 2\pi - \delta \}.
\end{aligned} \tag{87}$$

where $R \gg 1$ and $\epsilon \ll 1$ are free parameters, and $tg(\delta) = \frac{\epsilon}{R}$. Along this contour the function f_m can have complex values, and hence we define

$$\Lambda \equiv Re[f_m] \quad ; \quad \phi \equiv Im[f_m]. \tag{88}$$

The integral can thus be written as

$$Z_M(L, M; \beta) = \frac{1}{2\pi i A^3} \oint_{C_{bc}} dz_+ e^{-L[\Lambda(m, z_+; \beta) + i\phi(m, z_+; \beta)]}. \tag{89}$$

The contribution of part (II) of C_{bc} is $O(\epsilon)$ and hence can be neglected in the limit $\epsilon \rightarrow 0$. To show the same for part (IV) we note that for $|u| \gg 1$, $|\Phi_\gamma(u)| \sim \log(u)^\gamma$. Hence from (44) we see that for $|z_+| = R \gg 1$, $z_-^* \sim (\log R)^{-\gamma}$. Hence along part (IV) the absolute value of the integrand scales as $(R^{-L} \log(R)^{\gamma L})$ which vanishes faster than R^{-2} for any extensive L_+ and therefore the integral over (IV) is zero. Hence only parts (I) and (III) contribute.

The polylogarithm function, and hence also f_m , has a series expansion with real coefficients. Therefore $f_m(m, \bar{z}; \beta) = \overline{f_m(m, z; \beta)}$ where \bar{z} is the complex conjugate of z . Parts (I) and (III) traverse complex conjugated paths (in reverse order) and hence

$$Z_M(L, M; \beta) = \frac{1}{\pi A^3} \int_{1+i0}^{\infty+i0} dz_+ e^{-L\Lambda} \sin(L\phi). \tag{90}$$

This integral can be handled by a version of the stationary phase approximation: If $\frac{d}{dz}\phi(m, z; \beta) \neq 0$, the rapid oscillations of the $\sin()$ function (due to the large L) would imply that the neighborhood of z has no contribution to the integral. For $z = 1$, $\frac{d}{dz}\phi(m, z; \beta) = 0$, and due to the factor z_+^{-L+} it will be the only extremum contributing. Hence the integral can be limited to a small neighborhood $(1, \eta)$, i.e.

$$Z_M(L, M; \beta) \approx \frac{1}{\pi A^3} \int_1^{1+\eta} dz_+ e^{-L\Lambda} \sin(L\phi), \quad (91)$$

where η will be set shortly. It is shown below (section B.1) that

$$\Lambda(m, 1 + \delta z; \beta) \approx \Lambda(m, 1; \beta) + b_\Lambda(m; \beta) \delta z, \quad (92)$$

$$\phi(m, 1 + \delta z; \beta) \approx b_\phi(m; \beta) \delta z^{\beta C - 1}. \quad (93)$$

Inserting (92-93) into (91) yields

$$\begin{aligned} Z_M(L, M; \beta) &\approx \frac{e^{-L\Lambda(m, 1; \beta)}}{\pi A^3} \int_0^\eta d\delta z e^{-Lb_\Lambda \delta z} \sin(Lb_\phi \delta z^{\beta C - 1}) \\ &= \frac{e^{-L\Lambda(m, 1; \beta)}}{\pi A^3 L b_\Lambda} \int_0^{b_\Lambda L \eta} du e^{-u} \sin\left(\frac{L b_\phi}{(b_\Lambda L)^{\beta C - 1}} u^{\beta C - 1}\right). \end{aligned}$$

As there is no saddle point for $z_+ < 1$, and $f_m(m, z \rightarrow 0; \beta) \rightarrow -\infty$, we see that $b_\Lambda > 0$. In addition, Eq.(93) together with the condition $L\phi(m, 1 + \eta; \beta) = 1$ implies $\eta \sim L^{\frac{1}{1-\beta C}}$. In the thermodynamic limit the upper limit tends to infinity as $\beta C > 2$. In addition, due to e^{-u} factor only $u = O(1)$ contributes, and in this region the argument of the $\sin()$ tends to 0 (as $\beta C > 2$), hence it can be expanded:

$$\begin{aligned} Z_M(L, M; \beta) &\approx \frac{e^{-L\Lambda(m, 1; \beta)} b_\phi}{\pi A^3 L^{\beta C - 1} b_\Lambda^{\beta C - 2}} \int_0^\infty du e^{-u} u^{\beta C - 1} \\ &= \frac{b_\phi \Gamma(\beta C)}{\pi A^3 L^{\beta C - 1} b_\Lambda^{\beta C - 2}} e^{-L f_m(m, 1; \beta)}. \end{aligned}$$

Q.E.D

B.1. Deriving Eqs.(92-93)

We wish to prove (92-93). We define $z_-^*(1 + \delta) = z_-^*(1) + \chi$. Then Eq.(44) implies

$$\Phi_{\beta C}(z_-^*(1) + \chi) = \frac{1}{A^2 \Phi_{\beta C}(1 + \delta)}.$$

Expanding both sides in terms of χ and δ for $\beta C > 2$ yields

$$\begin{aligned} \Phi_{\beta C}(z_-^*(1) + \chi) &\approx \Phi_{\beta C}(z_-^*(1)) + \frac{1}{z_-^*} \Phi_{\beta C - 1}(z_-^*(1)) \chi, \\ \frac{1}{\Phi_{\beta C}(1 + \delta)} &\approx \frac{1}{\zeta_{\beta C} + \zeta_{\beta C - 1} \delta + i\pi \delta^{\beta C - 1} / \Gamma(\beta C)} \\ &\approx \frac{1}{\zeta_{\beta C}} - \frac{\zeta_{\beta C - 1}}{\zeta_{\beta C}^2} \delta - i \frac{\pi}{\zeta_{\beta C}^2 \Gamma(\beta C)} \delta^{\beta C - 1}. \end{aligned}$$

Hence

$$\begin{aligned} \text{Re}[\chi] &= - \frac{\zeta_{\beta C - 1} z_-^*(1)}{A^2 \zeta_{\beta C}^2 \Phi_{\beta C - 1}(z_-^*(1))} \delta + o(\delta), \\ \text{Im}[\chi] &= - \frac{\pi z_-^*(1)}{\Phi_{\beta C - 1}(z_-^*(1)) A^2 \zeta_{\beta C}^2 \Gamma(\beta C)} \delta^{\beta C - 1} + o(\delta^{\beta C - 1}). \end{aligned}$$

Inserting these results into the definition of f_m , i.e. Eq.(45), yields

$$\begin{aligned}
f_m(m, 1 + \delta; \beta) &= \frac{1+m}{2} \log(1 + \delta) + \frac{1-m}{2} \log(z_-^* + \chi) \\
&\approx \frac{1-m}{2} \log(z_-^*) + b_\Lambda(m; \beta) \delta - i b_\phi(m; \beta) \delta^{\beta c - 1}, \\
b_\Lambda(m; \beta) &= \frac{1+m}{2} - \frac{(1-m) \zeta_{\beta c - 1} \Phi_{\beta c}(z_-^*)}{2 \zeta_{\beta c} \Phi_{\beta c - 1}(z_-^*)}, \\
b_\phi(m; \beta) &= \frac{\pi(1-m)}{\Phi_{\beta c - 1}(z_-^*) A^2 \zeta_{\beta c}^2 \Gamma(\beta c)},
\end{aligned}$$

with $z_-^* = z_-^*(1)$. Hence

$$\begin{aligned}
\Lambda(m, 1 + \delta) &\approx \Lambda(1) + b_\Lambda(m; \beta) \delta, \\
\phi(m, 1 + \delta) &\approx b_\phi(m; \beta) \delta^{\beta c - 1}.
\end{aligned}$$

Q.E.D

C. Approximating (54) without saddle point

Here we calculate the integral (54) when $f_n(n, z)$ has no saddle point for $|z| < 1$, i.e. in the regime $n < n_c$, which implies $\beta C > 2$. This case is very similar to the case considered in Appendix B, and hence we skip some of the details. The contour of the integral can be deformed to a contour C_{bc} , defined by Eq.(87) and presented in Fig.9b. Along this contour the function f_n can have complex values, and hence we define

$$\Lambda \equiv \text{Re}[f_n] \quad ; \quad \phi \equiv \text{Im}[f_n].$$

The integral then can be written in a form equivalent to (89-90)

$$\begin{aligned}
Z_N(L, Ln; \beta) &= \frac{1}{2\pi i} \oint_{C_{bc}} dz e^{-L[\Lambda(n, z; \beta) + i\phi(n, z; \beta)]} \\
&\approx \frac{1}{\pi} \int_1^{1+\eta} dz e^{-L\Lambda} \sin(L\phi),
\end{aligned}$$

where as above $\eta \ll 1$. Following similar steps to those done in section B.1, one can find

$$\Lambda(n, 1 + \delta z; \beta) \approx \Lambda(n, 1; \beta) + b_\Lambda \delta z, \quad (94)$$

$$\phi(n, 1 + \delta z; \beta) \approx b_\phi \delta z^{\beta C - 1}. \quad (95)$$

with

$$\begin{aligned}
b_\Lambda &= 1 - \frac{n \zeta_{\beta c - 1}}{\zeta_{\beta c}}, \\
b_\phi &= n \frac{\pi}{\Gamma(\beta c) \zeta_{\beta c}}.
\end{aligned}$$

As $n < n_c = \zeta_{\beta c} / \zeta_{\beta c - 1}$ this implies $b_\Lambda > 0$ as expected. Following the same steps as in appendix B this implies

$$\begin{aligned}
Z_N(L, Ln; \beta) &\approx \frac{e^{-L\Lambda(n, 1; \beta)}}{\pi} \int_0^\eta d\delta z e^{-L b_\Lambda \delta z} \sin(L b_\phi \delta z^{\beta C - 1}) \\
&\approx \frac{b_\phi \Gamma(\beta C)}{\pi L^{\beta C - 1} b_\Lambda^{\beta C}} e^{-L f_n(n, 1; \beta)}.
\end{aligned} \quad (96)$$

D. Numerical procedure for evaluating the partition function

Here we explain the numerical procedure that is used to evaluate $Z_M(L, M; \beta)$ exactly. The partition function Z_M , with the boundary conditions $\sigma_1 = 1$ and $\sigma_L = -1$, which we denote by $(+-)$, has the form

$$\begin{aligned} Z_M^{(+ -)}(L, M; \beta) &= \sum_{\nu=1}^{\infty} \sum_{l_1=1}^{\infty} \dots \sum_{l_N=1}^{\infty} e^{-\beta\Delta(2\nu-1)} \left(\prod_{a=1}^{2\nu} \frac{1}{l_a^{\beta C}} \right) I \left(L = \sum_{a=1}^{2\nu} l_a \right) I \left(M = - \sum_{a=1}^{2\nu} (-1)^a l_a \right) \\ &= \sum_{l_1=1}^{\infty} \frac{e^{-\beta\Delta}}{l_1^{\beta C}} \sum_{\nu=1}^{\infty} \sum_{l_2=1}^{\infty} \dots \sum_{l_N=1}^{\infty} e^{-\beta\Delta(2\nu-2)} \left(\prod_{a=2}^{2\nu-1} \frac{1}{l_a^{\beta C}} \right) \\ &\quad \times I \left(L = l_1 + \sum_{a=2}^{2\nu-1} l_a \right) I \left(M = l_1 - \sum_{a=2}^{2\nu-1} (-1)^a l_a \right) \\ &= \sum_{l_1=1}^{\infty} \frac{e^{-\beta\Delta}}{l_1^{\beta C}} Z_M^{(- -)}(L - l_1, M - l_1; \beta), \end{aligned}$$

where $Z_M^{(- -)}$ is the partition function corresponding to boundary conditions $s_1 = s_L = -1$ (so that the number of domains is odd). A similar analysis for $Z_M^{(- -)}$ reads

$$\begin{aligned} Z_M^{(- -)}(L, M; \beta) &= \sum_{\nu=1}^{\infty} \sum_{l_1=1}^{\infty} \dots \sum_{l_N=1}^{\infty} e^{-\beta\Delta(2\nu-2)} \left(\prod_{a=1}^{2\nu-1} \frac{1}{l_a^{\beta C}} \right) I \left(L = \sum_{a=1}^{2\nu-1} l_a \right) I \left(M = \sum_{a=1}^{2\nu-1} (-1)^a l_a \right) \\ &= \sum_{l_1=1}^{\infty} \frac{e^{-\beta\Delta}}{l_1^{\beta C}} \sum_{\nu=1}^{\infty} \sum_{l_2=1}^{\infty} \dots \sum_{l_N=1}^{\infty} e^{-\beta\Delta(2\nu-3)} \left(\prod_{a=2}^{2\nu-2} \frac{1}{l_a^{\beta C}} \right) \\ &\quad \times I \left(L = l_1 + \sum_{a=2}^{2\nu-2} l_a \right) I \left(M = -l_1 + \sum_{a=2}^{2\nu-2} (-1)^a l_a \right) \\ &= \sum_{l_1=1}^{\infty} \frac{e^{-\beta\Delta}}{l_1^{\beta C}} Z_M^{(+ -)}(L - l_1, M + l_1; \beta). \end{aligned}$$

Hence we deduce the following coupled recursion relations

$$Z_M^{(+ -)}(L, M; \beta) = \sum_{l=1}^{\frac{L+M}{2}} \frac{e^{-\beta\Delta}}{l^{\beta C}} Z_M^{(- -)}(L - l, M - l; \beta), \quad (97)$$

$$Z_M^{(- -)}(L, M; \beta) = \sum_{l=1}^{\frac{L-M}{2}} \frac{e^{-\beta\Delta}}{l^{\beta C}} Z_M^{(+ -)}(L - l, M + l; \beta). \quad (98)$$

The total chain size L reduces in each step of applying these relations, and hence convergence is guaranteed. The base of the recursion is

$$\forall L : \quad Z_M^{(+ -)}(L, \pm(L-2); \beta) = \frac{e^{-\beta\Delta}}{(L-1)^{\beta C}}, \quad (99)$$

$$\forall L : \quad Z_M^{(- -)}(L, -L; \beta) = \frac{1}{L^{\beta C}}. \quad (100)$$

- [1] Bar A and Mukamel D 2014 *Phys. Rev. Lett.* **112** 015701
- [2] Fisher M E and Berker A N 1982 *Phys. Rev. B* **26** 2507
- [3] Anderson P W and Yuval G 1969 *Phys. Rev. Lett.* **23** 89–92

- [4] Thouless D 1969 *Phys. Rev.* **187** 732–733
- [5] Dyson F J 1971 *Comm. Math. Phys.* **21** 269–283
- [6] Cardy J L 1981 *J. Phys. A: Mathematical and General* **14** 1407
- [7] Aizenman M, Chayes J, Chayes L and Newman C 1988 *J. Stat. Phys.* **50** 1–40
- [8] Slurink J and Hilhorst H 1983 *Physica A: Statistical Mechanics and its Applications* **120** 627–634
- [9] Poland D and Scheraga H A 1966 *J. Chem. Phys.* **45** 1456–1463
- [10] Fisher M E 1966 *J. Chem. Phys.* **45** 1469
- [11] Blossey R and Indekeu J O 1995 *Phys. Rev. E* **52** 1223
- [12] Fisher M E 1984 *J. Stat. Phys.* **34** 667–729
- [13] Gross D, Kanter I and Sompolinsky H 1985 *Phys. Rev. Lett.* **55** 304–307
- [14] Toninelli C, Biroli G and Fisher D S 2006 *Phys. Rev. Lett.* **96** 035702
- [15] Toninelli C, Biroli G and Fisher D 2007 *Phys. Rev. Lett.* **98** 129602
- [16] Schwarz J, Liu A J and Chayes L 2006 *Europhys. Lett.* **73** 560
- [17] Liu Y Y, Csóka E, Zhou H and Pósfai M 2012 *Phys. Rev. Lett.* **109** 205703
- [18] Liu W, Schmittmann B and Zia R 2012 *Europhys. Lett.* **100** 66007
- [19] Zia R, Liu W and Schmittmann B 2012 *Phys. Procedia* **34** 124–127
- [20] Tian L and Shi D N 2012 *Phys. Lett. A* **376** 286–289
- [21] Bizhani G, Paczuski M and Grassberger P 2012 *Phys. Rev. E* **86** 011128
- [22] Sheinman M, Sharma A and MacKintosh F 2014 *arXiv:1402.0907*
- [23] Anderson P W, Yuval G and Hamann D 1970 *Phys. Rev. B* **1** 4464
- [24] Kafri Y, Mukamel D and Peliti L 2000 *Phys. Rev. Lett.* **85** 4988
- [25] Kosterlitz J M and Thouless D J 1973 *J. Phys. C: Solid State Physics* **6** 1181
- [26] Ruelle D 1968 *Comm. Math. Phys.* **9** 267–278
- [27] Dyson F J 1969 *Comm. Math. Phys.* **12** 91–107
- [28] Fröhlich J and Spencer T 1982 *Comm. Math. Phys.* **84** 87–101
- [29] Luijten E and Blöte H W 1997 *Phys. Rev. B* **56** 8945
- [30] Luijten E and Meßingfeld H 2001 *Phys. Rev. Lett.* **86** 5305
- [31] Touchette H 2009 *Phys. Rep.* **478** 1–69
- [32] Lee T and Yang C N 1952 *Phys. Rev.* **87** 410–419
- [33] Blythe R and Evans M 2003 *Barz. J. Phys.* **33** 464–475
- [34] Evans M R and Hanney T 2005 *J. Phys. A: Mathematical and General* **38** R195
- [35] Kafri Y, Mukamel D and Peliti L 2002 *The European Physical Journal B-Condensed Matter and Complex Systems* **27** 135–146
- [36] Bar A, Kabakçoğlu A and Mukamel D 2011 *Phys. Rev. E* **84** 041935
- [37] Huang K 1987 *Statistical Mechanics* (John Wiley & Sons)
- [38] Guinea F, Hakim V and Muramatsu A 1985 *Phys. Rev. Lett.* **54** 263–266
- [39] Meyer C 2000 *Matrix analysis and applied linear algebra book and solutions manual* vol 2 (Siam)
- [40] Achlioptas D, D'Souza R M and Spencer J 2009 *Science* **323** 1453–1455
- [41] da Costa R A, Dorogovtsev S N, Goltsev A V and Mendes J F F 2010 *Phys. Rev. Lett.* **105** 255701
- [42] Bray A 1994 *Adv. Phys.* **43** 357–459
- [43] Lee B P and Cardy J L 1993 *Phys. Rev. E* **48** 2452